

Distinct sulfur saturation histories within the Palaeogene Magilligan Sill, Northern Ireland: Implications for Ni-Cu-PGE mineralisation in the North Atlantic Igneous Province

Jordan J. Lindsay*¹, Hannah S. R. Hughes^{1, 2}, Dermot Smyth³, Iain McDonald⁴, Adrian J. Boyce⁵, Jens C. Ø. Andersen¹

¹ Camborne School of Mines, College of Engineering Mathematics and Physical Sciences, University of Exeter, Penryn Campus, Penryn, Cornwall, TR10 9EZ, UK.

(*jl731@exeter.ac.uk)

² School of Geosciences, University of the Witwatersrand, Private Bag 3, Wits 2050, Johannesburg, South Africa

³ Lonmin (Northern Ireland) Ltd., 6 Plasketts Close, Kilbegs Business Park, Kilbegs Road, ANTRIM, Northern Ireland, BT41 4LY, UK

⁴ School of Earth and Ocean Sciences, Cardiff University, Park Place, Cardiff, CF10 3AT, UK

⁵ Scottish Universities Environmental Research Centre (SUERC), East Kilbride, Glasgow, Scotland, G75 0QF, UK

The ~60 m thick Magilligan Sill is part of the British Palaeogene Igneous Province in the North Atlantic. The sill comprises layers of dolerite and olivine gabbro, and it intrudes a thick sequence of Mesozoic mudstones and marls, which are locally baked at the sill margins. Since 2014, the sill has been an exploration target for orthomagmatic Ni-Cu-PGE sulfide mineralisation analogous to the Noril'sk-Talnakh intrusion in Russia. We present new petrological, geochemical and S-isotope data to assess the prospectivity of the sill and the underlying magmatic plumbing system. Most sulfides in the dolerite portions of the sill are < 50 μm in size and comprise only pyrite with PGE abundances below detection limit. In the olivine gabbros, > 150 μm size pentlandite, chalcopyrite and pyrrhotite grains contain < 4 ppm total PGE, 1 460 ppm Co and 88 ppm Ag. Pyrite from the dolerites have $\delta^{34}\text{S}$ ranging from -10.0 to +3.4 ‰ and olivine gabbro sulfides range from -2.5 to -1.1 ‰, suggesting widespread crustal contamination. The S/Se ratios of sulfides in the dolerites and olivine gabbros range from 3 500 to 19 500 and from 1 970 to 3 710, respectively, indicating that the latter may have come from upstream in the magma plumbing system. The Magilligan Sill records multiple injections of mafic magma into an inflating sill package, each with distinct mechanisms towards S-saturation. Whilst the sulfide minerals in the sill do not constitute significant mineralisation themselves, detailed in-situ studies highlight a divergence in S-saturation histories, and suggest that a larger volume of olivine gabbro sulfides at depth may be prospective.

Keywords: PGE, sulfur isotopes, magma conduit system, mineralisation, North Atlantic Igneous Province

1 **Introduction**

2 Mafic-ultramafic magmatic plumbing systems in the upper crust may be highly
3 prospective for orthomagmatic sulfide mineralisation, and they host some of the largest Ni–Cu
4 and platinum group element (PGE) deposits in the world such as at Noril’sk and at Pechenga
5 in Russia (Naldrett 1997). The formation of sulfide deposits in plumbing systems requires three
6 major mechanisms: 1) The emplacement of a relatively metal-rich, initially S-undersaturated
7 mantle-derived magma from depth; 2) S-saturation of magma (normally via assimilation of
8 crustal S) and subsequent separation of immiscible sulfide from the silicate melt, followed by
9 the partitioning of chalcophile elements into the sulfide liquid; 3) Accumulation of droplets of
10 sulfide liquid forming mineralisation potentially at an economic scale (Leshner and Burnham
11 2001, Maier 2005, Maier and Groves 2011, Barnes et al. 2015). Chalcophile elements,
12 including Ni, Cu and PGE, partition strongly into sulfide phases upon the formation of an
13 immiscible sulfide liquid in a S-saturated silicate magma (e.g. Campbell and Naldrett 1979,
14 Crocket 2002, Naldrett 2004, 2010, Barnes and Lightfoot 2005). The mass ratio of silicate melt
15 interacting with sulfide liquid is described by an ‘R-factor’ and the mass of magma exchanging
16 siderophile metals with sulfide liquid has a strong influence on final ore composition (Campbell
17 and Naldrett 1979, Lightfoot 2007). A cumulative R-factor may be envisaged whereby
18 replenishment of a conduit system by multiple magma batches progressively upgrades the
19 sulfide tenor by allowing sulfide liquid to interact with and receive metal from large volumes
20 of silicate melt (Kerr and Leitch 2005). This process is shown to be instrumental in creating
21 conduit-hosted orthomagmatic Ni-Cu-PGE deposits such as within the Noril’sk Talnakh
22 intrusion in Russia (Barnes et al. 2016), the Platreef of the Bushveld Complex (e.g. Holwell
23 and McDonald 2007, Holwell et al. 2011, Ihlenfeld and Keays 2011), the Insizwa Complex of
24 South Africa (Lightfoot et al. 1984), and Voisey’s Bay in Canada (Huminicki et al. 2008).

25 A silicate melt can dissolve sulfur until it reaches the threshold of sulfur content at
26 sulfide saturation (SCSS; Shima and Naldrett 1975). Adding excess crustal sulfur via
27 assimilation may cause a magma to exceed the SCSS, and melting of country rock sulfides can
28 directly introduce a sulfide xenomelt into the magma (Leshner 2017). Changing the pressure,
29 temperature, and/or oxidation state of the magma can also shift the SCSS. In either case this
30 forces the magma to exsolve an immiscible sulfide liquid (Mavrogenes and O'Neill 1999). The
31 S-isotopic composition of sulfide minerals (e.g., $\delta^{34}\text{S}$) in high degree mantle melts is near
32 chondritic, while sulfides in crustal rocks are more isotopically variable (Faure 1977). Mantle
33 $\delta^{34}\text{S}$ is typically $0.1 \pm 0.5 \text{ ‰}$ (Sakai et al. 1984), and values different from this indicate
34 assimilation of crustal rock in a magma. A second tool for analysing the causes for sulfide
35 saturation is the S/Se ratio of sulfides. Contrasts in S/Se are often much larger and more
36 sensitive than $\delta^{34}\text{S}$. In the absence of crustal contamination, sulfides in mantle-derived magmas
37 will have $\text{S/Se} < 4,000$ (Lorand et al. 2003, Lorand and Alard 2010) with typical 'mantle-like'
38 S/Se ratios ranging from 2 850 to 4 350 (Eckstrand and Hulbert 1987). Divergence from the
39 average mantle ranges of $\delta^{34}\text{S}$ and S/Se indicates contamination of the magma by crustal sulfur
40 or partial oxidation of the sulfide minerals after crystallisation. Sulfur-saturation can occur
41 multiple times and at different depths in conduit systems (e.g. Li et al. 2009, Hayes et al. 2015),
42 and thus studies using geochemical proxies and indicators for the causes of S-saturation must
43 take this into account. Hence, a combination of $\delta^{34}\text{S}$ and S/Se can be used to produce a more
44 complete picture of the triggers for S-saturation (including R-factor; Leshner and Burnham
45 2001) and as an exploration vectoring tool towards mineralisation in orthomagmatic systems
46 (Queffurus and Barnes 2015, Smith et al. 2016).

47 Platinum-group minerals (PGM) and small-scale sulfide mineralisation is documented
48 on the Isles of Skye, Mull and Rum (Butcher et al., 1999; Pirrie et al., 2000; Power et al., 2000,
49 as reviewed by Hughes, 2015) in the Scottish portion of the British Palaeogene Igneous

50 Province (BPIP). The region is part of the North Atlantic Igneous Province (NAIP), an area
51 that has been highlighted as potentially prospective for orthomagmatic PGE mineralisation
52 (Andersen et al., 2002). Recent studies on the islands of Skye and Rum have also highlighted
53 extensive contamination of shallow Palaeogene intrusions by crustal S from Mesozoic
54 sediments (Power et al. 2003, Hughes et al. 2015a, 2016), exemplified by light S-isotopic
55 compositions of steeply dipping conduits (e.g. Hughes et al. 2015). By comparison, little
56 research has been carried out on orthomagmatic mineralisation and S sources in the Irish
57 portion of the BPIP.

58 The Magilligan Sill is a mafic intrusion on the north coast of County Londonderry,
59 Northern Ireland. It crops out close to the western edge of the Antrim Plateau, and is part of
60 the BPIP. While the Magilligan Sill has never been dated, ^{40}Ar – ^{39}Ar geochronology for the
61 nearby Portrush Sill estimates an age of 54.9 ± 0.6 Ma (McKenna 2009). We speculate that the
62 two sills are of comparable ages given their lithological similarity and their emplacement
63 beneath the Antrim lavas and into Mesozoic sediments. Given its setting within a large igneous
64 province, injected through a thick sequence of S-rich crustal sediments, the Magilligan Sill
65 became an exploration target for Lonmin (Northern Ireland) Ltd, who investigated the site from
66 2014 to 2017. This paper presents the first detailed account of the petrology and geochemistry
67 of the Magilligan Sill. We use sulfide-specific and bulk rock S-isotope compositions together
68 with *in situ* sulfide major and trace element analyses of Lonmin borehole core samples from
69 the sill to establish the causes of S-saturation in magma batches prior to emplacement into the
70 intrusion. We use this to assess the prospectivity of the sill itself as well as that of the
71 surrounding magmatic plumbing system, using Noril'sk as an analogue.

72 **Regional Geology**

73 The North Atlantic Igneous Province formed during a period of continental flood basalt
74 magmatism as the proto-Icelandic mantle plume impinged upon the thick continental
75 lithosphere under the North Atlantic and Rae Cratons, and adjoining orogenic belts.
76 Continental flood basalt magmatism (both tholeiitic and alkalic) initiated c. 62 Ma across what
77 is now Greenland and Baffin Island, and the UK and Ireland (in the form of the BPIP), and
78 associated rifting ultimately led to the opening of the Atlantic Ocean (Saunders et al. 1997).
79 BPIP lavas were erupted over a timespan of approximately 3 Myr (61-58 Ma; White and Lovell
80 1997). Several volcanic disconformities within the now eroded lava fields (Single and Jerram
81 2004) juxtapose lava batches that were fed by multiple volcanic centres or fissure systems
82 (Jerram and Widdowson 2005).

83 *Palaeogene lavas*

84 In Northern Ireland, the geology of County Antrim and the eastern edge of County
85 Londonderry is dominated by onshore lava fields of the BPIP. Along with the Isles of Skye and
86 Mull in Scotland, Antrim hosts some of the best-preserved examples of Palaeogene flood
87 basalts in the North Atlantic region (Wilson 1972, Kerr 1997). The Antrim Plateau lavas cover
88 roughly 3 800 km² and are stratigraphically separated into the tholeiitic Lower and Upper
89 Basalt Formations (Lyle and Patton 1989) – Figure 1. The up to 531 m thick Lower Basalts
90 were erupted at 62.6 ± 0.6 Ma (Ganerød et al. 2011). They become more intermediate in
91 composition up-sequence (Lyle and Patton 1989), including isolated interbasaltic rhyolite
92 extrusions in the Tardree Mountains in the centre of the Lower Basalts (Ganerød et al. 2011).
93 The up to 346 m thick Upper Basalts were erupted at 59.6 ± 0.6 Ma and they mark a return to
94 more primitive compositions (Ganerød et al. 2011).

95 The thickest and most extensive lava field in the Scottish portion of the BPIP on the
96 Isle of Mull is estimated to be 1800 m thick, covering approximately 840 km² (Emeleus and

97 Bell, 2005). In contrast to the Antrim lavas, the Mull Lavas have been divided into three
98 principal groups (in chronological order; the transitional tholeiitic-alkalic Mull Plateau Group,
99 the Coire Gorm type lavas, and the Central Mull Tholeiites) according to the petrogenetic and
100 geochemical characterisation of Kerr (1993, 1995). For the Antrim lavas, it has been postulated
101 that the reappearance of tholeiitic mafic magma was the product of a later, more extensive
102 melting event within the proto-Icelandic plume source (Lyle 1985, 1988). However, a more
103 recent interpretation of the changing magmatic regime of the plume, as represented by the Mull
104 lavas, was proposed by Kerr (1993, 1995) and Kerr et al. (1999) who identified a change from
105 small degrees of partial melting of a deeper, garnet-bearing mantle source to progressively
106 higher degrees of partial melting of a shallower and depleted spinel-bearing mantle.

107 ***Palaeogene magma plumbing systems***

108 Palaeogene igneous intrusions are emplaced into most levels of the Mesozoic
109 stratigraphy in Northern Ireland. NW-SE trending dyke swarms detected by magnetic surveys
110 occur under much of the Antrim Plateau (GSNI 2004), and are analogous to those observed in
111 the Scottish portions of the BPIP. Dolerite sills intrude Mesozoic sedimentary rocks exposed
112 along the north Antrim coast, including the Portrush and Magilligan Sills (Wilson 1972) (Fig.
113 1). The Portrush Sill is the more studied of these two intrusions, with work published on its
114 petrology and country rock contact metamorphism (Ledevin et al. 2012). The Portrush Sill
115 comprises a highly altered olivine gabbro with thin aphanitic chilled margins. As the sill
116 intruded, it baked the surrounding Jurassic siltstones to cordierite hornfels facies for ~10 m
117 from the intrusion margins (Ledevin *et al.*, 2012). It is younger than the Antrim Plateau Lavas
118 (54.9 ± 0.6 Ma; McKenna, 2009), consists of a main sill with two smaller sills above it, and is
119 estimated to be 45-60 m thick. Unlike intrusions at Noril'sk or Pechenga, the Portrush Sill is
120 thought not to have fed a large volume of magma to the surface.

121 The Magilligan Sill (Fig. 1, 2), first documented in the subsurface via drilling during a
122 Mineral Reconnaissance Programme drilling campaign (BGS 1964), has rarely been mentioned
123 in the literature. Wilson (1983) describes it as a ~60 m thick dolerite sill emplaced into Jurassic
124 Lias mudstones, which are underlain by Triassic and Permian sediments (Fig. 2). There is no
125 published geochronological or geochemical data available for the sill.

126 By contrast, there is an abundance of published literature on the petrology and
127 magmatic development of the Trotternish Sills and Shiant Sill (Fig. 1) of the Isle of Skye and
128 Shiant Isles, respectively (Scottish BPIP). Like the Magilligan and Portrush Sills, the
129 Trotternish Sills and Shiant Sill are not contemporaneous with the adjoining lava field (Skye
130 lava field). The Trotternish Sills are 250 m thick, comprising individual sub-alkaline intrusions,
131 up to 130 m thick (Gibson 1990). The sills contain ‘fingers’ or horizons of picrites,
132 picrodolerites and crinanites, many of which have chilled margins (Gibson and Jones 1991).
133 The Shiant Sill lies further west and is more alkaline than the Trotternish Sills, but is similar in
134 thickness and also contains multiple intrusive units (Gibson and Jones 1991). The Shiant Sill
135 is dominated by crinanites and picrodolerites with infrequent metre-thick picrite horizons (Gibb
136 and Henderson 1984). The sills in both localities are thought to have formed from discrete
137 pulses of differentiating alkali-basalt magma being injected into the sill from a single,
138 chemically zoned chamber beneath the sill complex (Gibson and Jones 1991). The geology of
139 the Magilligan, Portrush and Trotternish Sills is compared in Figure 3.

140 ***Mesozoic sedimentary basin***

141 The Palaeogene intrusions were emplaced into sedimentary rocks of the British
142 Hebridean basin and as such, the country rocks are similar in both Northern Ireland and
143 Scotland. The Magilligan and Portrush Sills in Northern Ireland intrude the Lower Jurassic
144 Waterloo Mudstone Formation of the Lower Lias Group (GSNI 2004), whereas the Trotternish

145 Sill intrudes the Middle Jurassic Lealt Shale and Valtos Sandstone Formations of the Great
146 Estuarine Group (Woodcock and Strachan 2012) (Fig. 3). The Shiant Sill intrudes Lower Lias
147 Group sediments, a large raft of which separates the intrusion into two bodies that were
148 previously thought to be distinct (Gibb and Henderson 1984). Intermittent evaporite horizons
149 are common within the Mesozoic northern British basin (GSNI 2004). The entire Mesozoic
150 succession in Britain represents a S-rich source that could have contaminated and assimilated
151 Palaeogene intrusions.

152 **Geology of the Magilligan Sill**

153 The Magilligan Sill has a chilled upper margin of aphyric to very fine-grained, normally
154 olivine-deficient dolerite, present in all exploration boreholes, below which is a 5 m thick zone
155 of vesicular fine-grained dolerite (Fig. 4). The sill coarsens gradually to become a gabbro 10-
156 20 m from the intrusion margin, with rare olivine identified in the majority of the drill core.
157 Green-tinged (more olivine-rich), 1-5 m thick layers, that are distinct from the dark grey
158 gabbros, occur sporadically throughout the sill. Within the bottom 10 m of the sill, the grain
159 size decreases progressively to form a lower chilled dolerite margin with abundant vesicles in
160 the lowermost 1-2 m. Rafts of baked sediment occur within the intrusion, and < 1 m isolated
161 zones of dolerite occur within the country rock outside the main intrusion. Multiple layers of
162 dolerite/gabbro form individual units in the intrusive sequence (Fig. 4). Each unit coarsens
163 downwards and displays a range of crystal sizes across their thickness, but overall the centre
164 of the sill is significantly coarser than the margins. The country rock surrounding the sill
165 comprises mudstone with occasional phosphatic and sandy units, and is notably baked and
166 metamorphosed to hornfels in the 1-3 m immediately next to the sill contact. Outwith the baked
167 contacts, the mudstones are dark grey, fissile and pyrite-rich. Proximal to the sill, baked
168 mudstones are very fine grained, cordierite facies slates with visible fine pyrite.

169 **Methodology**

170 A total of forty-seven half or quarter diamond drill core samples were collected for this
171 study from three Lonmin boreholes that intersect the sill and the overlying and underlying
172 Mesozoic sedimentary rocks. These boreholes are referred to here as “Boreholes 1, 2 and 3”,
173 and their locations are shown in Figure 2. Table A1 (see Supplementary Material) gives a full
174 list of hand specimen descriptions for all drill core samples.

175 ***Microscopy and mineral analysis***

176 Transmitted and reflected light optical microscopy was undertaken at Camborne School
177 of Mines (CSM), University of Exeter, using a Nikon Eclipse E600 Pol microscope with Nikon
178 Digital Sight 5MP camera on 12 polished thin sections prepared from the Magilligan Sill drill
179 core samples and its country rocks.

180 Quantitative mineral analysis was undertaken on eight of the polished thin sections of
181 the sill samples at CSM with a JEOL JXA-8200 Electron Microprobe (EPMA), using a
182 Wavelength Dispersive Spectrometer (WDS). Silicate and sulfide standards were used to
183 calibrate for major elements Si, Na, Cr, K, Al, Mg, Mn, Ca, Fe, Ni, Zn, Ti and V, and Fe, S,
184 Ni, Pb, Co and Cu, respectively. Standard analyses and results are shown in Table S1 (silicates
185 and sulfides) (see Supplementary Material). The beam parameters were 15 nÅ, at 15 kV for
186 thin section samples 1, 5, 6 and 7, and 1 nA at 20 kV for thin section samples 2, 3, 8, and 10.
187 Major elements (Si, Na, K, Al, Mg, Mn, Ca, Fe, S) had counting times of 20 s peak and 10 s
188 background, while minor/trace elements (Cr, Ni, Zn, Ti, V, Pb, Co, Cu) were 30 s peak and 15
189 s background. Backscattered electron images were taken separately using the same instrument.

190 ***LA-ICP-MS***

191 Laser ablation inductively coupled plasma mass spectrometry (LA-ICP-MS) was
192 undertaken at the School of Earth and Ocean Sciences, Cardiff University, on polished thin

193 sections using a New Wave Research UP213 UV laser system with a Thermo X Series 2 ICP-
194 MS. Laser analyses were utilised in order to investigate the trace element content of individual
195 sulfide grains *in situ* within samples, with the beam moving across mineral surfaces linearly.
196 The beam size was 40 μm , using a 10 Hz current with a power of $\sim 6 \text{ Jcm}^{-2}$ and an average
197 ablation rate of $6 \mu\text{ms}^{-1}$ along a programmed linear route. Acquisition times ranged from 70 to
198 150 s, with longer times for larger sulfides (according to laser line length), with an additional
199 40 s per acquisition to accommodate gas blank measurement and chamber flushing/evacuation.
200 Calibration was conducted using three in-house sulfide standards of known compositions
201 developed at Cardiff University (for further details see Prichard et al. 2013, Smith et al. 2014).
202 Major elements ^{57}Fe , ^{61}Ni and ^{65}Cu , and trace elements ^{59}Co , ^{66}Zn , ^{75}As , ^{77}Se , ^{95}Mo , $^{99,101}\text{Ru}$,
203 ^{103}Rh , $^{105,106,108}\text{Pd}$, ^{109}Ag , ^{111}Cd , ^{121}Sb , ^{125}Te , ^{185}Re , ^{189}Os , ^{193}Ir , ^{195}Pt , ^{197}Au , ^{206}Pb and ^{209}Bi
204 were calibrated using these standards. Sulfur concentrations were assumed based on sulfide
205 mineralogy. Following calibration, the Memorial Pyrrhotite Po724 standard was run as an
206 unknown to check machine accuracy. An internal pyrite standard was analysed as a qualitative
207 comparison for stoichiometric S values of pyrite, pyrrhotite, pentlandite and chalcopyrite. The
208 results of each stage of calibration are shown in Table S2 (see Supplementary Material).

209 ***Sulfur isotopes***

210 Sulfur isotope analyses were undertaken at the Scottish Universities Environmental
211 Research Centre (SUERC), University of Glasgow. A representative subset of six sill samples
212 and five sediment samples were selected for conventional sulfur isotope analysis. Individual
213 sulfide crystals were handpicked from within sedimentary samples for analysis. Sill samples
214 were crushed using a standard jaw crusher, sieved and manually ground into a powder, with as
215 little silicate material as possible. 5 mg of each powdered sample was added to 200 mg of CuO
216 powder (for a single analysis) and the compound was homogenised using a mortar and pestle,
217 and stored in a glass pellet. For sill samples, due to the small sulfide size, a Frantz Magnetic

218 Barrier Lab Separator was used to separate most of the silicate minerals, retaining the sulfides
219 (mainly the paramagnetic pyrrhotite) for blending with the CuO powder. The compound
220 samples were then combusted in their glass pellets at 1020 °C, and the gas emitted was
221 extracted into a vacuum line. Water was frozen off in acetone and dry ice, and SO₂ and CO₂
222 were separated by a multistage freeze-thaw system using liquid nitrogen and N-pentane. SO₂
223 was collected at the end of the process, and detected by a ThermoFisher Scientific MAT 253
224 dual inlet mass spectrometer. The spectrometer measures the abundance of ³⁴S and ³²S in the
225 gas, giving a relative ratio of the two isotopes ($\delta^{34}\text{S}$). The ratio was compared to an in-house
226 SO₂ gas standard of known $\delta^{34}\text{S}$. The raw $\delta^{34}\text{S}$ was then calibrated using the Vienna Canyon
227 Diablo Troilite (VCDT) global $\delta^{34}\text{S}$ standard for sulfur isotope analysis, and results reported in
228 ‰ relative to the VCDT. Multiple runs of two powdered international standards (chalcopyrite
229 CP-1, -4.56 ‰; sphalerite NBS-123, +17.1 ‰) and one in-house standard (silver sulfide IAEA-
230 S-3, -32.2 ‰) were analysed using the conventional sulfur gas extraction line as unknowns
231 prior to sample analysis to test calibration accuracy. Standard analyses were repeated twice to
232 establish data precision. Standard calibration results and sample repeats are shown in Table S3
233 (see Supplementary Material).

234 **Results**

235 *Petrology*

236 The locations of thin section samples T1-12 with respect to Boreholes 1-3 are shown in
237 Figure 4. Dolerites at the topmost sill contact (e.g., T1, 4, 5 and 6) generally have a very fine-
238 grained almost aphanitic groundmass (<100 μm), and are primarily composed of subophitic
239 semi-chloritized augite and anorthite (highly altered to zeolites and clays), with infrequent
240 olivine phenocrysts (completely or partially serpentinised or chloritized). Dolerites below this
241 ~2 m chilled margin contain 200 to 700 μm diameter zeolite-quartz-calcite-filled vesicles over

242 a depth interval of approximately 5 m. The lowermost contact of the sill (T10 and 12) is
243 texturally and mineralogically similar to the top one, with a 1 m thick chilled margin and a 3
244 m thick vesicular zone. Augite, anorthite and altered olivine phenocrysts dominate the very
245 fine-grained groundmass. Chlorite is abundant, not only partially replacing mafic minerals but
246 also appearing interstitially, in fractures, and as part of the matrix. In the top and lower sill
247 contacts, small spinels (<500 μm and ranging titanomagnetite to ilmenite) make up >5% of the
248 rock.

249 Inwards from the contact zones, the sills become coarser (mm-scale crystals) and thus
250 are classed as gabbros. However, individual segments of the sill package vary considerably in
251 their mineralogy – for example, T2 and 3 of Borehole 3 are simply coarser versions of the rocks
252 found at the top contact of the sill (gabbros), whereas T7 and 8 of Borehole 1 are distinct with
253 a notably higher olivine content (olivine gabbros). The olivine gabbros in the core (observed
254 in mainly in Borehole 1, with sub-metre thick sections in Borehole 3) have their own chilled
255 margins (10-20 cm thick) and glassier olivine crystals at the edge. In general, clinopyroxene
256 and plagioclase are the major components of all gabbros (40-50 % and 25-40 % respectively).
257 Olivine gabbros contain >30 % olivine, which is reasonably fresh and with minor iddingsite
258 within fractures (Fig. 5a). Olivine found in gabbros (5-10 % of their composition) is always
259 serpentinised (Fig. 5b). Orthopyroxene occurs in T2 only with an abundance of < 5 %. As seen
260 in the chilled margins, spinels in the central portions of the sill are an intricate mix of
261 titanomagnetite and ilmenite (and equigranular with surrounding groundmass silicates, on a
262 millimetre-scale).

263 Sulfide minerals are observed with variable abundances throughout all units and
264 lithologies in the sill. The upper and lower contact zones and the coarser gabbro sections of the
265 sill host trace (<1 %) interstitial small grains (averaging $\sim 50 \mu\text{m}$) of pyrite and pyrrhotite only
266 (Fig. 5c). Chalcopyrite and bornite (<70 μm) are found in very rare instances. By contrast, the

267 olivine gabbro units contain a mixture of sulfides (generally >150 μm) in higher proportions
268 (1-2 %) including pyrite, pyrrhotite, chalcopyrite, pentlandite, and galena – normally in
269 complex intergrowths (Fig. 5d). Sulfides in the olivine gabbros are often partially oxidised
270 (10-20 % around rims) with skeletal grain shapes due to dissolution. In comparison, sulfides in
271 the gabbros are generally fresher (< 5 % surface alteration). No platinum group minerals (PGM)
272 are observed in the samples.

273 ***Mineral chemistry***

274 *Silicates*

275 The major element compositions of clinopyroxenes in the sill are distinct between
276 gabbros and olivine gabbros (Fig. 6a-b) – the olivine gabbros contain magnesian and/or calcic
277 pyroxenes (14.0-15.5 wt. % MgO, 22.0-22.5 wt. % CaO and 5-7 wt. % FeO), whereas all other
278 pyroxenes are more iron-rich (7-11 wt. % FeO, with 12-14 wt. % MgO and 20.5-22.0 wt. %
279 CaO). As such, olivine gabbro clinopyroxenes are less augitic, with Mg, Ca, Fe, and Al bearing
280 varieties found in T7 and 8. Individual pyroxenes in the olivine gabbros are often
281 compositionally zoned. Olivine in olivine gabbros have Fo% of ~65 compared to ~50 in
282 (unserpentinised) olivine in other sill lithologies. Plagioclase is systematically more anorthitic
283 in olivine gabbros with mean An% of 82, compared to 70 in the gabbros. A full list of major
284 element concentrations can be found in Supplementary Table S4.

285 *Sulfides*

286 A summary of major and trace element compositions of sulfides from the Magilligan
287 Sill and surrounding country rocks obtained from LA-ICP-MS are presented in Table 1, with
288 the full list displayed in Supplementary Material Table S2. Figures 7a-d summarise the trace
289 element geochemistry of sulfides found in the Magilligan Sill. Cobalt is concentrated in olivine
290 gabbro sulfides, with the highest amounts (< 2 700 ppm) found in pentlandite; the average Co

291 concentration across all olivine gabbro sulfides above detection is 1 460 ppm. Silver is present
292 between 2.3 and 315 ppm in olivine gabbro sulfides (highest in pentlandite, although also
293 present in chalcopyrite), with an average of 88 ppm across all olivine gabbro sulfides above
294 detection. Sulfides excluding those in the olivine gabbros contain < 0.12 ppm Re, < 570 ppm
295 Co and < 5.3 ppm Ag. Figures 7a and 7b show a slight positive correlation between Ni
296 concentrations and Co/Ag concentrations in sulfides. The PGE are below detection in pyrite
297 from dolerites (from the upper and lower contact zones) and gabbros throughout the sill
298 package. By contrast, sulfides in the olivine gabbros contain up to 4 ppm total palladium-group
299 PGE (PPGE; Rh, Pt and Pd), and up to 0.24 ppm iridium-group PGE (IPGE; Os, Ir and Ru). In
300 T7 and 8, Ru and Rh are only found in chalcopyrite grains (average of 0.2 and 0.65 ppm,
301 respectively). The remaining PGE are found in both chalcopyrite and pentlandite (Fig. 7c-d):
302 Pd is more abundant in chalcopyrite (0.25 – 2.43 ppm); Pt is more abundant in pentlandite (0.03
303 – 0.66 ppm); and Os and Ir have been recorded close to background in both minerals between
304 0.02 and 0.05 ppm. Rhenium is also more abundant in olivine gabbro chalcopyrite and
305 pentlandite than pyrite from other gabbros and dolerites (0.04 – 0.96 ppm compared to a
306 maximum of 0.12 ppm, respectively). The absence of visible PGM suggests that PGE are found
307 within sulfide structures.

308 Selenium concentrations for Magilligan sulfides are plotted against Ni and total PGE
309 concentrations (from Table S2, Supplementary Material) in Figures 8a-c. Olivine gabbro
310 sulfides have Se concentrations between 91 and 171 ppm, with S/Se ratios between 1 980 and
311 3 720. Sulfides in the remainder of the sill have Se concentrations between 21 and 95 ppm (if
312 above the detection limit), and S/Se ratios ranging from 3 510 to 25 200. Sulfides in the local
313 sediment have Se concentrations between 49 and 99 ppm, and S/Se ratios of between 5 390
314 and 10 800. In a comparison between S/Se and total PGE concentrations (Fig. 8c),
315 chalcopyrites in the olivine gabbros tend to have S/Se ratios of 1 980 – 3 340 and total PGE

316 concentrations of 0.6 – 3.7 ppm. Pyrrhotites and pentlandites are similar in terms of S/Se (~ 2
317 700–3 700), but pentlandite tends to have higher total PGE (< 2.5 ppm). The absence of the
318 highest S/Se values in Fig. 8a-c reinforces the fact that sulfides with high S/Se (e.g. gabbros,
319 marginal dolerites and sediment) have, in almost all cases, no detectable PGE or Ni.

320 *Sulfur isotope compositions*

321 A summary of $\delta^{34}\text{S}$ compositions for the Magilligan Sill and surrounding country rock
322 is shown in Table 2 (full dataset in Supplementary Table S3) and Figure 9a. Mesozoic shales
323 adjacent to the sill have $\delta^{34}\text{S}$ values ranging from -10 to +5.3 ‰ above the intrusion and from
324 -20.4 to -14.9 ‰ below it. Dolerites at the intrusion edge have $\delta^{34}\text{S}$ values between -9.6 and -
325 2.5 ‰, whereas gabbros are consistently +3.4 ‰. Olivine gabbros have $\delta^{34}\text{S}$ values from -2.5
326 to -1.1 ‰.

327 Combined $\delta^{34}\text{S}$ and S/Se data (from the LA-ICP-MS dataset) are displayed in Figure
328 9b. S/Se and $\delta^{34}\text{S}$ values of the sill and its surroundings can be compared to the magmatic norm
329 for each parameter. Only olivine gabbro samples overlap the ‘magmatic’ boundaries of S/Se (2
330 850-4 350; Eckstrand and Hulbert 1987, Queffurus and Barnes 2015) and $\delta^{34}\text{S}$ (0.1 ± 0.5 ‰;
331 Sakai et al. 1984), highlighted by the hatched square in Figure 9b. S/Se values for the olivine
332 gabbros and sediments are more restricted compared to the wide ranges observed in the
333 dolerites and gabbros. In general, sulfides in the dolerites and gabbros have S/Se ratios 2-5
334 times that of the maximum magmatic norm (up to 20 000 compared to less than ~4 000). Figure
335 10 presents a downhole log of the Magilligan Sill in terms of S/Se ratios, S isotopes and trace
336 element concentrations in sulfides. High PGE, Ni, Cu and Ag contents are confined to the
337 olivine gabbro sulfides only, and S/Se and $\delta^{34}\text{S}$ downhole trends appear to mirror each other.

338 **Discussion**

339 *Magmatic history of the Magilligan Sill*

340 The Magilligan Sill has a coarse gabbroic interior and chilled doleritic margins, fitting
341 well with descriptions of similar sills found within the BPIP – the Portrush Sill, of a similar
342 thickness and mafic petrology (Ledevin et al. 2012); and the thicker Trotternish Sills, with
343 distinct chemical changes throughout (Gibson 1990, Gibson and Jones 1991). As the magma
344 intruded the Mesozoic Waterloo mudstones (Fig. 11a), the outermost parts of the sill would
345 have cooled rapidly, resulting in the very fine-grained and vesicular dolerites seen in T1, 4, 5
346 and 6 (top), and T10 and 12 (bottom). Heat transfer from the sill would have simultaneously
347 metamorphosed country sediment to cordierite hornfels facies (Fig. 11b), in a similar fashion
348 to the Portrush Sill (Ledevin et al. 2012). Following intrusion, water from an external source,
349 potentially meteoric, altered olivine and plagioclase in the crystallised sill to produce hydrous
350 silicates (Fig. 11c). The inwards gradation to coarser grained rocks (T2 and 3) is observed in
351 all three boreholes, which contain similarly altered augite, anorthite, and titanomagnetite-
352 dominated compositions in all but the olivine gabbro samples that occur sporadically
353 throughout the sill. These olivine-rich portions (e.g. T7 and 8) feature large, reasonably fresh
354 olivine crystals, and are chemically and texturally distinct from the rocks found elsewhere in
355 the sill. Their pyroxenes are Mg- and Ca-rich as opposed to Fe-rich, their plagioclases are more
356 anorthitic than albitic, and they are less pervasively altered. The abrupt nature of the marked
357 downhole petrological changes from dolerite/gabbro to olivine gabbro indicates that the
358 variation is not gradational, and the presence of fine, glassy margins within olivine gabbro
359 sections implies that they were chilled against already solidified and cooled dolerites and
360 gabbros. Hence, we conclude that the olivine gabbros are formed from new pulses of primitive
361 magma emplaced into the earlier and already altered gabbro-dolerite sill to form distinct
362 olivine-rich horizons observed in the sill (Fig. 11d).

363 In the Magilligan Sill, the clinopyroxene-plagioclase dominated rocks are more altered
364 and superseded by fresher modal olivine melts, inconsistent with Bowen's discontinuous

365 reaction series, in which high temperature olivine crystallisation normally precedes
366 clinopyroxene and plagioclase crystallisation in a cooling system (Bowen 1979). The more
367 forsteritic olivine and anorthitic plagioclase in the olivine gabbros also suggest higher
368 temperature crystallisation. We suggest that the magmatic system was replenished by younger,
369 more primitive mantle melts following the initial emplacement of gabbros and dolerites, or that
370 the olivine-rich horizons were formed from a completely different magma. It is unlikely that
371 the entire magma source changed, given the localised nature of the sill, and thus re-introduction
372 of mafic melts into a deeper magma reservoir is the preferred scenario.

373 We envisage that the Magilligan Sill developed in a similar manner to the Trotternish
374 Sills. A stepwise decrease in MgO content throughout the petrological units of the Trotternish
375 Sills from oldest to youngest (40 % in picrites, 20-10 % in picrodolerites, and 5 % in crinanites)
376 reflects an evolving magma system with each unit injected in discontinuous pulses (Gibson
377 1990). The Skye lava field ranges in composition from basalt and picrobasalt to hawaiiite and
378 mugearite, also suggesting a differentiating source during Palaeogene volcanism (Hughes et al.
379 2015b). Internal chilled margins within the Trotternish Sills and Shiant Sill reinforce the idea
380 of multiple injections – these are also present within the Magilligan Sill. If a magma chamber
381 were replenished between units, subsequent magma compositions would be more mafic than
382 the previous one (provided the influx is volumetrically significant relative to the resident
383 magma). This is observed in the increasingly mafic, late-stage Mull lavas (Kerr 1997). The
384 presence of multiple magma injections within equivalent sills across the BPIP and the presence
385 of olivine in the centre of the Magilligan Sill suggests that they are formed by similar petrogenic
386 processes. The Antrim Plateau Lavas and the Magilligan Sill follow similar evolutionary trends
387 towards mafic (magnesian) compositions from Lower to Upper Basalts, and from gabbro to
388 olivine gabbro, respectively.

389 *S-saturation and the formation of sulfides*

390 Magmatic sulfides typically have $\delta^{34}\text{S}$ values of $0.1 \pm 0.5 \text{ ‰}$ (Sakai et al. 1984). Some
 391 modern studies of MORB lava sulfides suggest larger ranges (Eckardt 2001, Seal 2006, Labidi
 392 et al. 2012), but the original values presented by Sakai *et al* account for seafloor sulfate/sulfide
 393 fractionation and are thus more precise and reliable (Leshner 2017). The local pristine magmatic
 394 $\delta^{34}\text{S}$ signature of the Scottish BPIP has been found to be $-2.3 \pm 1.5 \text{ ‰}$ (Hughes et al. 2015a)
 395 based on the mean composition of the picritic Trotternish Sills (Hughes et al. 2015a), which is
 396 comparable with that of Icelandic basalts (Torssander 1989) and MORB (Labidi et al. 2012).
 397 The Magilligan Sill sulfides record values between -9.6 and -1.1 ‰ , and one sample (T2) has
 398 $+3.4 \text{ ‰}$. Sulfides in local sediments adjacent to the sill record average $\delta^{34}\text{S}$ values of -6.0 ‰
 399 (above the sill) and -17.7 ‰ (below the sill). It follows that most of the sill magmas have
 400 experienced some degree of crustal contamination, as the addition of isotopically light crustal
 401 sulfur from the Mesozoic country rocks will shift their primary magmatic sulfide signature
 402 (assumed to be -2.3 ‰ for the BPIP; Hughes *et al.*, 2015). Based on work on the Trotternish
 403 Sills (Hughes et al. 2015a), the proportion of sedimentary sulfur assimilated by the magma (f)
 404 can be calculated, using the observed $\delta^{34}\text{S}$ values achieved in the contaminated sill ($\delta^{34}\text{S}_{\text{mix}}$)
 405 using the following equation:

$$406 \quad \delta^{34}\text{S}_{\text{mix}} = \frac{\delta^{34}\text{S}_c X_{cf} + \delta^{34}\text{S}_m X_m (1-f)}{X_{cf} + X_m (1-f)}$$

407 Here, $\delta^{34}\text{S}_m$ and $\delta^{34}\text{S}_c$ are the S isotopic conditions of the uncontaminated magma (0
 408 ‰) and the local sediment, respectively (-20.4 to -9.9 ‰). X_m and X_c are the concentrations of
 409 S in the magma and sediment, respectively. Figure 12 shows a binary mixing model between
 410 the sill and sedimentary sulfur, based on the calculation above. The upper margin of the sill
 411 contains around 8 % sedimentary sulfur, whereas the lower margin contains only 1 %. Around
 412 0.8 % of the sulfur in the olivine gabbro samples comes from sedimentary sulfur, and the
 413 gabbro samples contain almost no sedimentary sulfur (0.05 %). It follows that the margins of
 414 the intrusion will have had a greater degree of crustal interaction and S assimilation. The

415 diffusion of volatiles at the margins of the hot intrusion could have promoted the transfer of S
416 both from and into the proximal sediment (Penniston-Dorland et al. 2008), while direct
417 assimilation of crust would provide larger abundances of S more rapidly (Robertson et al.
418 2015). Marginal dolerite $\delta^{34}\text{S}$ deviates strongly from ‘mantle-like’ values (Sakai et al. 1984).
419 Despite being the only positive magmatic sample, gabbro sample T2 appears too isotopically
420 heavy to have a purely magmatic signature. However, a small amount of evaporitic material
421 (known to be in the country rocks; Wilson, 1979) may be responsible for the anomalously
422 positive $\delta^{34}\text{S}$ value (e.g. Ripley et al. 2003).

423 The dominance of S isotope values less than -2.5 ‰ in sulfides in the intrusion
424 (Supplementary Table S3) indicate that widespread contamination by up to 8 % crustal sulfur
425 (Fig. 12) occurred in the ascending magma at varying depths in the underlying magma
426 plumbing system. Despite this reasonably consistent contamination signature, highly variable
427 sulfide S/Se ratios between olivine gabbros and the rest of the sill suggest that the history of
428 magma contamination in the Magilligan Sill is more complicated than S isotopes imply (Fig.
429 9b). With the exception of the olivine gabbros, all sill units have S/Se between 3 510 and 25
430 200, strongly skewed to higher values that are far removed from the mantle norm of 2 850-4
431 350 (Eckstrand and Hulbert 1987, Queffurus and Barnes 2015). Only the olivine gabbros (S/Se
432 ranging from 1 980 to 3 720) appear to have retained a ‘mantle-like’ sulfide S/Se signature,
433 despite crustal isotopic input. Modelling the Pd, Se and S/Se concentrations of olivine gabbro
434 and gabbro sulfides yields that they are likely to have had R-factors of around 500-1 000 and
435 10-100, respectively. Modelling results are shown in Supplementary Material S5 and use
436 methods described by Lesher and Burnham (1999).

437 If the sill lithologies represent separate magma pulses (e.g. Fig. 11), the S/Se
438 discrepancy may be the result of largely different degrees of contamination (which contradicts
439 $\delta^{34}\text{S}$ signatures in Fig. 9) or, more likely, different S-saturation processes in each pulse

440 (indicated by different R-factors). Olivine gabbro sulfides have evidently lost S (e.g. low S/Se)
441 which could be due to ‘cumulative R-factor’, a process described by Kerr and Leitch (2005).
442 Sulfide liquids formed during contamination-driven S-saturation in the ascending magma may
443 be cycled upwards in the plumbing system by subsequent magma pulses, towards their final
444 resting horizon (e.g. Hayes et al. 2015). This will subject them to multistage dissolution
445 upgrading, wherein the sulfides are partially dissolved during transportation, reducing their
446 volume and S content while retaining their chalcophile element concentrations (e.g. PGE and
447 Se) (e.g. Kerr and Leitch 2005, Naldrett 2010). We propose that olivine gabbro sulfides in the
448 Magilligan Sill formed in this manner.

449 It should be noted that S loss and low S/Se in sulfides could also be induced by post-
450 magmatic partial oxidation of sulfide minerals, unrelated to S-saturation events (Peck and
451 Keays 1990, Dunn 1997, Queffurus and Barnes 2015). While minor oxidation of sulfides is
452 observed in the olivine gabbros (10-20 %), oxidation is unlikely to explain the significantly
453 lower S/Se ratio of these sulfides in comparison to those in the rest of the sill. For example, if
454 a sulfide grain from a gabbro (initial S/Se = 10 600) undergoes 20% S loss, this would decrease
455 the S/Se to 7 610. In the olivine gabbros, the mean S/Se ratio is 2 940 and if this were to be
456 produced by oxidation of gabbro sulfides alone, it would require a S loss of 72%. Such
457 oxidation should leave clear and visible signs in the olivine gabbro sulfides (e.g. oxide
458 minerals), for which there is no evidence. We conclude that cumulative R-factor is the most
459 likely cause of ‘mantle-like’ S/Se ratios in the Magilligan Sill.

460 In contrast to sulfides in the olivine gabbros, the lack of detectable trace metals and
461 high S/Se in sulfides from the dolerites and gabbros of the sill (Fig. 10) may imply that this
462 generation of magma remained S-undersaturated throughout ascent, only forming sulfides very
463 locally when contaminated by crustal S from the Waterloo Mudstones at the level of final
464 emplacement. This would inhibit chalcophile sequestration and cumulative R-factor upgrading

465 via magma transportation (as envisaged for the olivine gabbro sulfides) (Robertson et al. 2015).
466 This shallow, local S-saturation model is similar to that predicted for basalt dykes on the Isle
467 of Skye (Hughes et al. 2015a). In this way, sulfide (pyrite) formation is akin to very late-stage
468 magmatic-hydrothermal sulfide formation – there was no circulation of sulfide liquid in the
469 magmatic intrusion or feeder and hence no opportunity to equilibrate with the host silicate
470 magma and its chalcophile element content, resulting in base/precious metal poor pyrite. If the
471 base/precious metal bearing second generation sulfides were cycled from upstream in the
472 plumbing system, they may be found in higher (potentially economic) abundances below or
473 adjacent to the Magilligan Sill horizon (e.g. ‘earlier’ in the system). The change in $\delta^{34}\text{S}$ in
474 Figure 10 could potentially represent a diffusion profile, in which the outer parts of the sill (e.g.
475 the dolerites) volatilise and assimilate the most crustal S, reflected in high S/Se and negative
476 $\delta^{34}\text{S}$ values that gradually shift to more S-poor values towards interior gabbros. Olivine gabbros
477 disrupt the profile trend, further supporting the hypothesis that they are of a separate injection
478 of magma and different saturation events. Although diffusion via contact metamorphism is a
479 slow process compared to direct crustal assimilation (Robertson et al. 2015), field evidence of
480 the Trotternish Sills report 50-200 cm baked margins of hardened country sediment with
481 minimal surviving sulfide minerals adjacent to the intrusions (e.g. Gibson and Jones 1991,
482 Hughes et al. 2015a). This feature strongly indicates S diffusion was important in triggering S-
483 saturation in Trotternish magmas. Given that there are hornfelsed margins immediately next to
484 the Magilligan Sill, we suggest similar processes could have contributed here too within a
485 comparable timescale.

486 *Magmatic model*

487 By combining the silicate and sulfide petrography and sulfide compositions, we
488 envisage a final two-stage development model for the Magilligan Sill (Fig. 13). In Stage A, S-
489 undersaturated magma from a deep magma reservoir was emplaced as a sill into the Waterloo

490 Mudstones. Significant contamination of the magma by crustal S only occurred at the current
491 level of emplacement, through contact with the Waterloo Mudstones. This contamination
492 occurred via volatilisation of S from the country rock due to contact metamorphism, or via S
493 addition by direct crustal assimilation. This process was so late-stage and localised that the
494 sulfides within the sill formed under magmatic-hydrothermal conditions. This means that no
495 significant transportation of the sulfide liquid took place within the magma, and little
496 chalcophile elements (for which we use Se as a proxy) entered the sulfide (leading to high S/Se
497 ratios from 3 510 to 25 200 and $\delta^{34}\text{S}$ of -9.6 to -2.5 ‰ in the dolerites and gabbros). As a result,
498 sulfides (pyrite and pyrrhotite) crystallising from the S-saturated magma did not sequester
499 chalcophile elements successfully (Naldrett 2010).

500 In the time between the Stage A and B, the dolerites and gabbros were hydrothermally
501 altered (perhaps synchronously with local S volatilisation and pyrite formation) to produce
502 abundant chlorite and clays, and altering olivine phenocrysts to serpentine. In Stage B (Fig.
503 13), the source composition of the magma supply in the conduit system shifted to a more
504 primitive composition so that subsequent magma replenishment in the Magilligan Sill formed
505 the olivine gabbros. S-saturation likely occurred earlier (perhaps deeper) in the magma
506 plumbing system, as indicated by the upgrading processes envisaged for sulfides in the olivine
507 gabbros. Evaporites and mudstones in the Triassic Mercia Mudstone Group or the Permian
508 Belfast Group hundreds of metres below the Magilligan Sill could perhaps have supplied
509 crustal S to Stage B magma, driving it to S-saturation deeper in the system (GSNI 2004).
510 Sulfides (including pyrite, pyrrhotite, chalcopyrite and pentlandite) that segregated from the
511 silicate melt in Stage B contain higher abundances of Ag (< 88 ppm), Co (< 1 460 ppm), and
512 PGE (< 4 ppm). We propose that these sulfides were originally mineralised ‘upstream’ in the
513 plumbing system that fed the Magilligan Sill. They were cycled through subsequent pulses of
514 second-generation magma before being entrained and emplaced into the Magilligan Sill. The

515 pre-existing dolerites and gabbros formed during Stage A most likely shielded this second pulse
516 of magma (Stage B) from further S absorption from the local country rocks, preventing dilution
517 or addition of late-stage magmatic-hydrothermal S.

518 In this way, the Magilligan Sill, unlike the Trotternish Sills, retains evidence for
519 multiple S-saturation events and pathways between various episodes of magmatic
520 replenishment, as represented by discrete silicate magma pulses. The Southern Feeder Dike
521 Complex of Victoria Island in Canada (part of the Franklin Large Igneous Province) has been
522 interpreted in a similar way, also featuring evidence of conduit-focused magma replenishment
523 and sulfide cycling at different depths in its plumbing system (Hayes et al. 2015). Given that
524 the second-generation sulfides contain PGE, Ni, Cu, Co, and Ag, a higher volume
525 concentration of *in situ* mineralisation of similar or higher tenor nearer the depth at which S-
526 saturation occurred could provide an interesting target for further exploration, despite the
527 Magilligan Sill itself being sub-economic. Since the relatively thin (compared to the southwest)
528 Carboniferous limestones in County Londonderry overlie Proterozoic Grampian basement and
529 both of these contain few S-rich lithologies (GSNI 2004), Permian and Triassic sediments
530 above these appear to be the most logical exploration target for Stage B sulfide-bearing
531 intrusions. Halite beds in the White Brae Mudstone Formation (Permian), sabkha mudstones
532 and halite beds in the Craiganee Formation (Middle Triassic) or dark mudstones in the
533 Westbury Formation (Upper Triassic) are all suitable crustal S contaminants (Wilson 1972). A
534 deeper level of the Magilligan plumbing system in contact with one of these units could
535 potentially be the S-saturation horizon for the olivine gabbro sulfides, and should be the key
536 exploration target for any further Ni-Cu-PGE investigations in the area.

537 **Conclusions**

538 The identification of discrete magmatic pulses within the Magilligan Sill indicate that
539 at least two chemically distinct magma generations were emplaced within a single intrusion.
540 These magma batches may have had significantly different S-saturation pathways and
541 correspondingly different mineralisation potentials. The first magmatic generation crystallised
542 to form most of the sill – olivine-deficient, highly altered dolerites and gabbros with barren
543 sulfide minerals. The second generation crystallised to form olivine gabbro horizons within
544 the pre-existing sill, and contained metal-enriched sulfides. In order to form younger, more
545 primitive magmas, the feeder chamber must have mixed with a new magma between the
546 emplacements of the two different units in the sill, in a similar fashion to the Antrim Plateau
547 Lavas, in which mafic Upper Basalts postdate less mafic Lower Basalts.

548 The S-isotope composition ($\delta^{34}\text{S}$) of the Magilligan Sill indicates that crustal S
549 contamination is present throughout the entire intrusion. S/Se ratios in second-generation
550 (olivine gabbro) sulfides are similar to that of published average ‘magmatic’ values of 2 850-4
551 350 (Eckstrand and Hulbert 1987, Queffurus and Barnes 2015), indicating a deeper S-
552 saturation event perhaps with smaller degrees of crustal contamination. For this reason, sulfides
553 found in the olivine gabbro sections of the sill are interpreted to have formed at depth before
554 being cycled upstream by later magma pulses. The possible controls on this deep S-saturation
555 include: the changing initial composition of the magma at source; the amount of sedimentary
556 S available to the magma via assimilation, and the degree of shielding from these sediments
557 enforced by pre-existing layers of the sill; and the geometry of the magmatic plumbing system.
558 Through a combined approach of S-isotopes, S/Se ratios and detailed petrography, the
559 pathways to S-saturation may be determined within plumbing systems and valuable
560 information fed back into the exploration industry with regards to vectoring towards
561 orthomagmatic sulfide mineralisation, both in the BPIP and more generally for large igneous
562 provinces.

563 **Acknowledgements**

564 The investigation of the sill was based on an exploration model devised by Mr Tom
565 Evans (Executive Manager, Exploration, Lonmin) and the mineral exploration programme was
566 organised and implemented by Dr Dermot Smyth (Project Manager, Lonmin). This research
567 project was devised based on discussions between Dr Smyth and Dr Hughes. The authors
568 would like to thank Gavyn Rollinson, Peter Frost, Joe Pickles, and Charlie Compton-Jones at
569 the Camborne School of Mines laboratory facilities for their guidance during SEM and EPMA
570 analyses. Thanks are also extended to Alison McDonald of the Scottish Universities
571 Environmental Research Centre (SUERC) for her assistance on sulfur isotope analysis, and to
572 Lonmin (Northern Ireland) Ltd. for access to core and previous studies on the sill. Walkabout
573 Resources are thanked for their support in publishing this paper and access to company data.
574 Finally, we thank Mike Leshner, Sandy Cruden and Marie-Claude Williamson for their thorough
575 and insightful reviewer contributions that significantly improved the quality of this article. JJJ
576 is sponsored by the Vice-Chancellor Scholarship at the University of Exeter.

577

578 **References**

- 579 Barnes, S.-J., and Lightfoot, P.C. 2005. Formation of magmatic nickel-sulfide ore deposits
580 and processes affecting their copper and platinum-group element contents. *Economic*
581 *Geology*, **100th Anni**: 179–213.
- 582 Barnes, S.J., Cruden, A.R., Arndt, N., and Saumur, B.M. 2016. The mineral system approach
583 applied to magmatic Ni–Cu–PGE sulphide deposits. *Ore Geology Reviews*, **76**: 296–
584 316. Elsevier B.V. doi:10.1016/j.oregeorev.2015.06.012.
- 585 Barnes, S.J., Mungall, J.E., and Maier, W.D. 2015. Platinum group elements in mantle melts
586 and mantle samples. *Lithos*, **232**: 395–417. Elsevier B.V.

- 587 doi:10.1016/j.lithos.2015.07.007.
- 588 BGS. 1964. Summary of progress of the Geological Survey of Great Britain and the Museum
589 of Practical Geology for the year 1963. HMSO, London.
- 590 Bowen, N.L. 1979. The Evolution of Igneous Rocks: Fiftieth Anniversary Perspectives.
591 *Edited By*H.S. Yoder. Princeton University Press.
- 592 Butcher, A.R., Pirrie, D., Prichard, H.M., and Fisher, P.C. 1999. Platinum-group
593 mineralization in the Rum layered intrusion, Scottish Hebrides, UK. *Journal of the*
594 *Geological Society*, **156**: 213–216. doi:10.1144/gsjgs.156.2.0213.
- 595 Campbell, I.H., and Naldrett, A.J. 1979. The influence of silicate:sulfide ratios on the
596 geochemistry of magmatic sulfides. *Economic Geology*, **74**: 1503–1506.
- 597 Crocket, J.H. 2002. Platinum-group element geochemistry of mafic and ultramafic rocks. In:
598 *Geology, geochemistry, mineralogy and mineral beneficiation of platinum-group*
599 *elements, Canadian Institute of Mining, Metallurgy and Petroleum, Special Vol*: 177–
600 210.
- 601 Dunn, J.G. 1997. The oxidation of sulphide minerals. *Thermochim. Acta*, **300**: 127–139.
602 doi:10.1016/S0040-6031(96)03132-2.
- 603 Eckardt, F. 2001. The origin of sulphates: an example of sulphur isotopic applications.
604 *Progress in Physical Geography*, **25**: 512–519. doi:10.1191/030913301701543163.
- 605 Eckstrand, O.R., and Hulbert, L.J. 1987. Selenium and the source of sulfur in magmatic
606 nickel and platinum deposits. *Geological Association of Canada –Mineralogical*
607 *Association Canada Program with Abstracts*, **12**: 40.
- 608 Faure, G. 1977. Principles of isotope geology. *Related Information: Smith and Wyllie*
609 *intermediate geology series*, **16**: Medium: X; Size: Pages: 475.
- 610 Ganerød, M., Chew, D.M., Smethurst, M.A., Troll, V.R., Corfu, F., Meade, F., and Prestvik,
611 T. 2011. Geochronology of the Tardree Rhyolite Complex, Northern Ireland:

- 612 Implications for zircon fission track studies, the North Atlantic Igneous Province and the
613 age of the Fish Canyon sanidine standard. *Chemical Geology*, **286**: 222–228. Elsevier
614 B.V. doi:10.1016/j.chemgeo.2011.05.007.
- 615 Gibb, F.G.F., and Henderson, C.M.B. 1984. The structure of the Shiant Isles Sill Complex,
616 Outer Hebrides. *Scottish Journal of Geology*, **20**: 21–29.
- 617 Gibson, S.A. 1990. The geochemistry of the Trotternish sills, Isle of Skye - crustal
618 contamination in the British Tertiary Volcanic Province. *Journal of the Geological*
619 *Society*, **147**: 1071–1081. doi:10.1144/gsjgs.147.6.1071.
- 620 Gibson, S.A., and Jones, A.P. 1991. Igneous Stratigraphy and Internal Structure of the Little
621 Minch Sill Complex, Trotternish Peninsula, Northern Skye, Scotland. *Geological*
622 *Magazine*, **128**: 51–66. doi:10.1017/S0016756800018045.
- 623 GSNI. 2004. *The Geology of Northern Ireland - Our Natural Foundation. In 2nd edition.*
624 *Edited By* W.I. Mitchell. Crown, Belfast.
- 625 Hayes, B., Bédard, J.H., Hryciuk, M., Wing, B., Nabelek, P., Macdonald, W.D., and
626 Lissenberg, C.J. 2015. Sulfide Immiscibility Induced by Wall-Rock Assimilation in a
627 Fault-Guided Basaltic Feeder System, Franklin Large Igneous Province, Victoria Island
628 (Arctic Canada). *Economic Geology*, **110**: 1697–1717.
- 629 Holwell, D.A., and McDonald, I. 2007. Distribution of platinum-group elements in the
630 Platreef at Overysel, northern Bushveld Complex: A combined PGM and LA-ICP-MS
631 study. *Contributions to Mineralogy and Petrology*, **154**: 171–190. doi:10.1007/s00410-
632 007-0185-9.
- 633 Holwell, D.A., McDonald, I., and Butler, I.B. 2011. Precious metal enrichment in the
634 Platreef, Bushveld Complex, South Africa: Evidence from homogenized magmatic
635 sulfide melt inclusions. *Contributions to Mineralogy and Petrology*, **161**: 1011–1026.
636 doi:10.1007/s00410-010-0577-0.

- 637 Hughes, H.S.R., Boyce, A.J., McDonald, I., Davidheiser-Kroll, B., Holwell, D.A.,
638 McDonald, A., and Oldroyd, A. 2015a. Contrasting mechanisms for crustal sulphur
639 contamination of mafic magma: evidence from dyke and sill complexes from the British
640 Palaeogene Igneous Province. *Journal of the Geological Society*, **172**: 443–458.
641 doi:10.1144/jgs2014-112.
- 642 Hughes, H.S.R., McDonald, I., Boyce, A.J., Holwell, D.A., and Kerr, A.C. 2016. Sulphide
643 sinking in magma conduits: Evidence from mafic-ultramafic plugs on rum and the wider
644 north atlantic igneous province. *Journal of Petrology*, **57**: 1–33.
645 doi:10.1093/petrology/egw010.
- 646 Hughes, H.S.R., McDonald, I., and Kerr, A.C. 2015b. Platinum-group element signatures in
647 the North Atlantic Igneous Province: Implications for mantle controls on metal budgets
648 during continental breakup. *Lithos*, **233**: 89–110. Elsevier B.V.
649 doi:10.1016/j.lithos.2015.05.005.
- 650 Huminicki, M.A.E., Sylvester, P.J., Lastra, R., Cabri, L.J., Evans-Lamswood, D., and Wilton,
651 D.H.C. 2008. First report of platinum-group minerals from a hornblende gabbro dyke in
652 the vicinity of the Southeast Extension Zone of the Voisey's Bay Ni-Cu-Co deposit,
653 Labrador. *Mineralogy and Petrology*, **92**: 129–164. doi:10.1007/s00710-007-0205-5.
- 654 Ihlenfeld, C., and Keays, R.R. 2011. Crustal contamination and PGE mineralization in the
655 Platreef, Bushveld Complex, South Africa: Evidence for multiple contamination events
656 and transport of magmatic sulfides. *Mineralium Deposita*, **46**: 813–832.
- 657 Jerram, D.A., and Widdowson, M. 2005. The anatomy of Continental Flood Basalt
658 Provinces: Geological constraints on the processes and products of flood volcanism.
659 *Lithos*, **79**: 385–405.
- 660 Kerr, A.C. 1993. Elemental evidence for an enriched small-fraction-melt input into Tertiary
661 Mull basalts, Western Scotland. *Journal of the Geological Society*, **150**: 763–769.

- 662 Kerr, A.C. 1995. The geochemistry of the Mull-Morvern Tertiary lava succession, NW
663 Scotland: an assessment of mantle sources during plume-related volcanism. *Chemical*
664 *Geology*, **122**: 43–58. doi:10.1016/0009-2541(95)00009-B.
- 665 Kerr, A.C. 1997. The geochemistry and significance of plugs intruding the Tertiary Mull-
666 Morvern lava succession, western Scotland. *Scottish Journal of Geology*, **33**: 157–167.
667 doi:10.1144/sjg33020157.
- 668 Kerr, A.C., and Leitch, A.M. 2005. Self-destructive sulfide segregation systems and the
669 formation of high-grade magmatic ore deposits. *Economic Geology*, **100**: 311–332.
670 doi:10.2113/gsecongeo.100.2.311.
- 671 Labidi, J., Cartigny, P., Birck, J.L., Assayag, N., and Bourrand, J.J. 2012. Determination of
672 multiple sulfur isotopes in glasses: A reappraisal of the MORB $\delta^{34}\text{S}$. *Chemical*
673 *Geology*, **334**: 189–198. Elsevier B.V. doi:10.1016/j.chemgeo.2012.10.028.
- 674 Ledevin, M., Arndt, N.T., Cooper, M., Earls, G., Lyle, P., Auborg, C., and Lewin, E. 2012.
675 Intrusion history of the Portrush Sill, County Antrim, Northern Ireland: evidence for
676 rapid emplacement and high-temperature contact metamorphism. *Geology Magazine*,
677 **149**: 67–79.
- 678 Leshner, C.M. 2017. Roles of xenomelts, xenoliths, xenocrysts, xenovolatiles, residues, and
679 skarns in the genesis, transport, and localization of magmatic Fe-Ni-Cu-PGE sulfides
680 and chromite. *Ore Geology Reviews*, **90**: 465–484. Elsevier.
681 doi:10.1016/j.oregeorev.2017.08.008.
- 682 Leshner, C.M., and Burnham, O.M. 1999. Mass balance and mixing in dynamic ore-forming
683 magmatic systems. *In Dynamic Processes in Magmatic Ore Deposits and their*
684 *Application in Mineral Exploration. Edited by R.R. Keays, C.M. Leshner, P.C. Lightfoot,*
685 *and C.E.G. Farrow. Geological Association of Canada Short Course Notes. pp. 413–449.*
- 686 Leshner, C.M., and Burnham, O.M. 2001. Multicomponent elemental and isotopic mixing in

- 687 Ni-Cu-(PGE) ores at Kambalda, Western Australia. *Canadian Mineralogist*, **39**: 421–
688 446. doi:10.2113/gscanmin.39.2.421.
- 689 Li, C., Ripley, E.M., and Naldrett, A.J. 2009. A new genetic model for the giant Ni-Cu-pge
690 sulfide deposits associated with the siberian flood basalts. *Economic Geology*, **104**:
691 291–301. doi:10.2113/gsecongeo.104.2.291.
- 692 Lightfoot, P.C. 2007. Advances in Ni-Cu-PGE Sulphide Deposit Models and Implications for
693 Exploration Technologies. *Ore Deposits and Exploration Technology, Proceedings of*
694 *Exploration 07: Decennial International Conference on Mineral Exploration*, **Paper 44**:
695 629–646.
- 696 Lightfoot, P.C., Naldrett, A.J., and Hawkesworth, C.J. 1984. The geology and geochemistry
697 of the Waterfall Gorge section of the Insizwa complex with particular reference to the
698 origin of the nickel sulfide deposits. *Economic Geology*, **79**: 1857–1879.
699 doi:10.2113/gsecongeo.79.8.1857.
- 700 Lorand, J.P., and Alard, O. 2010. Determination of selenium and tellurium concentrations in
701 Pyrenean peridotites (Ariege, France): New insight into S/Se/Te systematics of the upper
702 in mantle samples. *Chemical Geology*, **278**: 120–130. Elsevier B.V.
703 doi:10.1016/j.chemgeo.2010.09.007.
- 704 Lorand, J.P., Alard, O., Luguet, A., and Keays, R.R. 2003. Sulfur and selenium systematics
705 of the subcontinental lithospheric mantle: Inferences from the Massif Central xenolith
706 suite (France). *Geochimica et Cosmochimica Acta*, **67**: 4137–4151. doi:10.1016/S0016-
707 7037(03)00305-3.
- 708 Lyle, P. 1985. The petrogenesis of the Tertiary basaltic and intermediate lavas of northeast
709 Ireland. *Scottish Journal of Geology*, **21**: 71–84.
- 710 Lyle, P. 1988. The Geochemistry, Petrology and Volcanology of the Tertiary Lava
711 Succession of the Binevenagh-Benbraddagh Area of County Londonderry. *Irish Journal*

- 712 of Earth Sciences, **9**: 141–151. Available from <http://www.jstor.org/stable/30002481>.
- 713 Lyle, P., and Patton, D.J.S. 1989. The Petrography And Geochemistry Of The Upper Basalt
714 Formation Of The Antrim Lava Group In Northeast Ireland. Irish Journal of Earth
715 Sciences, **1019477**: 33–41. Available from <http://www.jstor.org/stable/30002247>.
- 716 Maier, W.D. 2005. Platinum-group element (PGE) deposits and occurrences: Mineralization
717 styles, genetic concepts, and exploration criteria. Journal of African Earth Sciences, **41**:
718 165–191. doi:10.1016/j.jafrearsci.2005.03.004.
- 719 Maier, W.D., and Groves, D.I. 2011. Temporal and spatial controls on the formation of
720 magmatic PGE and Ni-Cu deposits. Mineralium Deposita, **46**: 841–857.
721 doi:10.1007/s00126-011-0339-6.
- 722 Mavrogenes, J.A., and O'Neill, H.S.C. 1999. The relative effects of pressure, temperature and
723 oxygen fugacity on the solubility of sulfide in mafic magmas. Geochimica et
724 Cosmochimica Acta, **63**: 1173–1180. doi:10.1016/S0016-7037(98)00289-0.
- 725 McKenna, J. 2009. The age and petrogenesis of Palaeogene flood basalt volcanism in NE
726 Ireland. 52nd Annual Irish Geological Research Meeting, February 2009,.
- 727 Naldrett, A.J. 1997. Key factors in the genesis of Noril'sk, Sudbury, Jinchuan, Voisey's Bay
728 and other world-class Ni-Cu-PGE deposits: implications for exploration. Australian
729 Journal of Earth Sciences, : 283–315.
- 730 Naldrett, A.J. 2004. Magmatic Sulfide Deposits. *In* Springer Berlin Heidelberg.
731 doi:10.1180/minmag.1990.054.377.28.
- 732 Naldrett, A.J. 2010. From the mantle to the bank: The life of a Ni-Cu-(PGE) sulfide deposit.
733 South African Journal of Geology, **113**: 1–32. doi:10.2113/gssajg.113.1-1.
- 734 Peck, D.C., and Keays, R.R. 1990. Insights into the Behaviour of Precious Metals in
735 Primitive, S-undersaturated Magmas: Evidence from the Heazlewood River Complex,
736 Tasmania. Canadian Mineralogist, **28**: 553–577.

- 737 Penniston-Dorland, S.C., Wing, B.A., Nex, P.A.M., Kinnaird, J.A., Farquhar, J., Brown, M.,
738 and Sharman, E.R. 2008. Multiple sulfur isotopes reveal a magmatic origin for the
739 Platreef platinum group element deposit, Bushveld Complex, South Africa. *Geology*, **36**:
740 979–982. doi:10.1130/G25098A.1.
- 741 Pirrie, D., Power, M.R., Andersen, J.C.Ø., and Butcher, a. R. 2000. Platinum-group
742 mineralization in the Tertiary Igneous Province: new data from Mull and Skye, Scottish
743 Inner Hebrides, UK. *Geological Magazine*, **137**: 651–658.
744 doi:10.1017/S0016756800004520.
- 745 Power, M.R., Pirrie, D., and Andersen, J.C.Ø. 2003. Diversity of platinum-group element
746 mineralization styles in the North Atlantic Igneous Province: new evidence from Rum,
747 UK. *Geological Magazine*, **140**: 499–512. doi:10.1017/S0016756803008045.
- 748 Power, M.R., Pirrie, D., Andersen, J.C.Ø., and Wheeler, P.D. 2000. Testing the validity of
749 chrome spinel chemistry as a provenance and petrogenetic indicator. *Geology*, **28**:
750 1027–1030. doi:10.1130/0091-7613(2000)28<1027:TTVOCS>2.0.CO;2.
- 751 Prichard, H.M., Knight, R.D., Fisher, P.C., McDonald, I., Zhou, M.-F., and Wang, C.Y.
752 2013. Distribution of platinum-group elements in magmatic and altered ores in the
753 Jinchuan intrusion, China: an example of selenium remobilization by postmagmatic
754 fluids. *Mineralium Deposita*, **48**: 767–786.
- 755 Queffurus, M., and Barnes, S.J. 2015. A review of sulfur to selenium ratios in magmatic
756 nickel-copper and platinum-group element deposits. *Ore Geology Reviews*, **69**: 301–
757 324. Elsevier B.V. doi:10.1016/j.oregeorev.2015.02.019.
- 758 Ripley, E.M., Lightfoot, P.C., Li, C., and Elswick, E.R. 2003. Sulfur isotopic studies of
759 continental flood basalts in the Noril'sk region: Implications for the association between
760 lavas and ore-bearing intrusions. *Geochimica et Cosmochimica Acta*, **67**: 2805–2817.
761 doi:10.1016/S0016-7037(03)00102-9.

- 762 Robertson, J., Ripley, E.M., Barnes, S.J., and Li, C. 2015. Sulfur liberation from country
763 rocks and incorporation in mafic magmas. *Economic Geology*, **110**: 1111–1123.
764 doi:10.2113/econgeo.110.4.1111.
- 765 Sakai, H., Marais, D.J.D., Ueda, A., and Moore, J.G. 1984. Concentrations and isotope ratios
766 of carbon, nitrogen and sulfur in ocean-floor basalts. *Geochimica et Cosmochimica*
767 *Acta*, **48**: 2433–2441. doi:10.1016/0016-7037(84)90295-3.
- 768 Saunders, A.D., Fitton, J.G., Kerr, A.C., Norry, M.J., and Kent, R.W. 1997. The North
769 Atlantic Igneous Province. *In Large Igneous Provinces: Continental, Oceanic and*
770 *Planetary Flood Volcanism. Edited by J.J. Mahoney and M. Coffin. American*
771 *Geophysical Union Monograph*. pp. 45–93. doi:10.1029/GM100p0045.
- 772 Seal, R.R. 2006. Sulfur Isotope Geochemistry of Sulfide Minerals. *Reviews in Mineralogy*
773 *and Geochemistry*, **61**: 633–677. doi:10.2138/rmg.2006.61.12.
- 774 Shima, H., and Naldrett, A.J. 1975. Solubility of sulfur in an ultramafic melt and the
775 relevance of the system Fe-S-O. *Economic Geology*, **70**: 960–967.
- 776 Single, R.T., and Jerram, D.A. 2004. The 3D facies architecture of flood basalt provinces and
777 their internal heterogeneity: examples from the Palaeogene Skye Lava Field. *Journal of*
778 *the Geological Society*, **161**.
- 779 Smith, J.W., Holwell, D.A., and McDonald, I. 2014. Precious and base metal geochemistry
780 and mineralogy of the Grasvalley Norite Pyroxenite Anorthosite (GNPA) member,
781 northern Bushveld Complex, South Africa: implications for a multistage emplacement.
782 *Mineralium Deposita*, **49**: 667–692. doi:10.1007/s00126-014-0515-6.
- 783 Smith, J.W., Holwell, D.A., McDonald, I., and Boyce, A.J. 2016. The application of S
784 isotopes and S/Se ratios in determining ore-forming processes of magmatic Ni-Cu-PGE
785 sulfide deposits: A cautionary case study from the northern Bushveld Complex. *Ore*
786 *Geology Reviews*, **73**: 148–174. The Authors. doi:10.1016/j.oregeorev.2015.10.022.

- 787 Torssander, P. 1989. Sulfur isotope ratios of Icelandic rocks. *Contributions to Mineralogy*
788 *and Petrology*, **102**: 18–23.
- 789 White, N., and Lovell, B. 1997. Measuring the pulse of a plume with the sedimentary record.
790 *Nature*, **387**: 888–891.
- 791 Wilson, H.E. 1972. *British Regional Geology - Northern Ireland. In 2nd edition. Edited*
792 *By*GSNI. H. M. Stationery Office, London.
- 793 Wilson, H.E. 1983. Deep Drilling in Northern Ireland since 1947. *The Irish Nationalists’*
794 *Journal*, **21**: 160–163.
- 795 Woodcock, N.H., and Strachan, R.A. 2012. *Geological History of Britain & Ireland. In 2nd*
796 *edition. Wiley-Blackwell, Oxford.*
- 797

Table 1 – Average LA-ICP-MS trace element concentrations of sulphides within upper and lower dolerites, gabbros, olivine gabbros and country sediment. * - calculated stoichiometrically. † - average concentration of detected isotopes. S = 53.45 wt. % \approx pyrite; S = 34.94 wt. % \approx chalcopyrite.

Lithology	S* Wt. %	S/Se	Fe Wt. %	Ni Wt. %	Cu Wt. %	Co ppm	Zn ppm	As ppm	Se ppm	Ru† ppm	Rh† ppm	Pd† ppm
U. Dolerite	53.45	14 279.29	48.60	0.19	0.04	535.455	510.54	19.40	43.32	-	-	-
Gabbro	53.45	10 635.11	44.37	-	0.05	100.70	241.80	20.67	56.21	-	-	-
O. Gabbro	34.94	2 943.03	48.72	6.86	9.26	1 454.59	3 922.32	-	122.89	0.1	0.33	0.64
L. Dolerite	53.45	11 595.33	52.54	0.33	0.10	727.30	3 492.78	355.99	44.79	-	-	-
Sediment	53.45	8117.503	45.02	0.10	0.07	594.90	117.55	1962.31	74.23	-	-	-

Sample	Ag ppm	Cd ppm	Sb ppm	Te ppm	Re ppm	Os ppm	Ir ppm	Pt ppm	Au ppm	Bi ppm	ΣPGE ppm
U. Dolerite	0.94	-	1.74	-	0.2	-	-	-	0.01	0.05	-
Gabbro	2.93	-	3.48	0.86	0.12	-	-	-	-	0.15	-
O. Gabbro	68.54	29.65	0.35	6.00	0.32	0.04	0.04	0.36	0.05	0.88	1.51
L. Dolerite	0.50	-	8.2	0.45	0.02	-	-	-	0.04	0.04	-
Sediment	6.38	0.86	85.59	6.38	0.06	-	-	0.05	0.91	0.65	0.05

Table 2 – Summary S-isotopic compositions of sill and country rock lithologies.

Lithology	Min $\delta^{34}\text{S}$ ‰	Max $\delta^{34}\text{S}$ ‰	Mean $\delta^{34}\text{S}$ ‰	n
Shale (above sill)	-10.00	+5.30	-5.95	4
Upper dolerite	-9.60	-2.50	-6.58	5
Gabbro	+3.40	+3.40	+3.40	2
Olivine Gabbro	-2.50	-1.10	-1.80	2
Lower Dolerite	-2.50	-2.50	-2.50	1
Shale (below sill)	-20.40	-14.90	-17.63	8
<i>Magilligan Sill</i>	-9.60	+3.40	+3.10	22
<i>(overall)</i>				

Figure Captions

Figure 1 – Schematic map of the geology of the BPIP, showing basement units, onshore lavas and notable intrusive complexes. Inset map gives the subdivisions of the Antrim Plateau lavas and the location of the Magilligan and Portrush Sills. Based on work by Woodcock and Strachan (2012).

Figure 2 – Schematic geological map of the Magilligan Peninsula, Northern Ireland, indicating the location of the Magilligan Sill and Boreholes 1-3.

Figure 3 – Simplified lithological logs of the Magilligan, Portrush and Trotternish Sills, with their relative intrusion level within the Jurassic stratigraphic columns for Scotland and Ireland. Sill packages are stylised to show multiple injection events. Formation names from Woodcock and Strachan (2012) and GSNI (2004). Portrush and Trotternish relationships from Ledevin (2012), and Gibson and Jones (1991), respectively.

Figure 4 – Representative composite geological log of the Magilligan Sill boreholes. "T" labels show the analysed thin section sample numbers and locations.

Figure 5 – Photomicrographs of Magilligan Sill thin sections: a) Olivine-deficient gabbro (T3) [transmitted light XPL]; b) Olivine gabbro (T7) [transmitted light XPL]; c) Small pyrite grains within gabbro (T2) [reflected light]; d) Large sulphide amalgamation within olivine gabbro, [back-scattered electron image, BSE] (T2). [Pl – plagioclase, Cpx – clinopyroxene, Ol – olivine, Py – pyrite, Po – pyrrhotite, Ccp – chalcopyrite, Pn – pentlandite, Gn – galena]

Figure 6 - Bivariate geochemical plots of a) MgO vs. CaO and b) MgO vs. FeO in analysed clinopyroxenes.

Figure 7 – Bivariate geochemical plots of sulphides in the Magilligan Sill: a) Ni vs. Co; b) Ni vs. Ag; c) Cu vs. total PGE; d) Fe vs. total PGE with respect to mineral phases. Gabbro samples do not contain detectable Ni or PGE.

Figure 8 – Bivariate geochemical plots of sulphides in the Magilligan Sill: a) Se vs. Ni/(Fe+Ni+Cu); b) Se vs. total PGE; c) S/Se vs. total PGE with respect to mineral phases.

Figure 9 – a) Histogram of $\delta^{34}\text{S}$ compositions of sulphides in the Magilligan Sill. b) Combined $\delta^{34}\text{S}$ vs. S/Se plot for sulphides in the Magilligan Sill, with published magmatic values from Seal (2006) and Quefferus and Barnes (2015). Crosshatched area represents typical magmatic/mantle values.

Figure 10 – Representative downhole variations in lithology (not to scale) combined with S/Se, $\delta^{34}\text{S}$, total PGE, Ni, Ag and Cu data from sulphides in these lithologies. Arrows on S/Se and $\delta^{34}\text{S}$ plots describe the suggested diffusion profile grading inwards from dolerite to gabbro.

Figure 11 – Petrological development of the Magilligan Sill, showing the two lithological phases found in the intrusion. [Pl – plagioclase, Cpx – clinopyroxene, Ol – olivine, Srp – serpentine, Chl – chlorite, Spl – spinel, Py – pyrite, Po – pyrrhotite, Ccp – chalcopyrite, Pn – pentlandite]

Figure 12 – Binary mixing model for the Magilligan Sill and sedimentary sulphur.

Figure 13 – Stage A in the magmatic development model for the Magilligan system, showing the formation of the dolerites and gabbros, and their barren sulphides. Stage B in the magmatic development model for the Magilligan system, showing the formation of the olivine gabbros, and their cycled base/precious metal sulphides. Model constructed with reference to similar systems in Barnes *et al.* (2016).

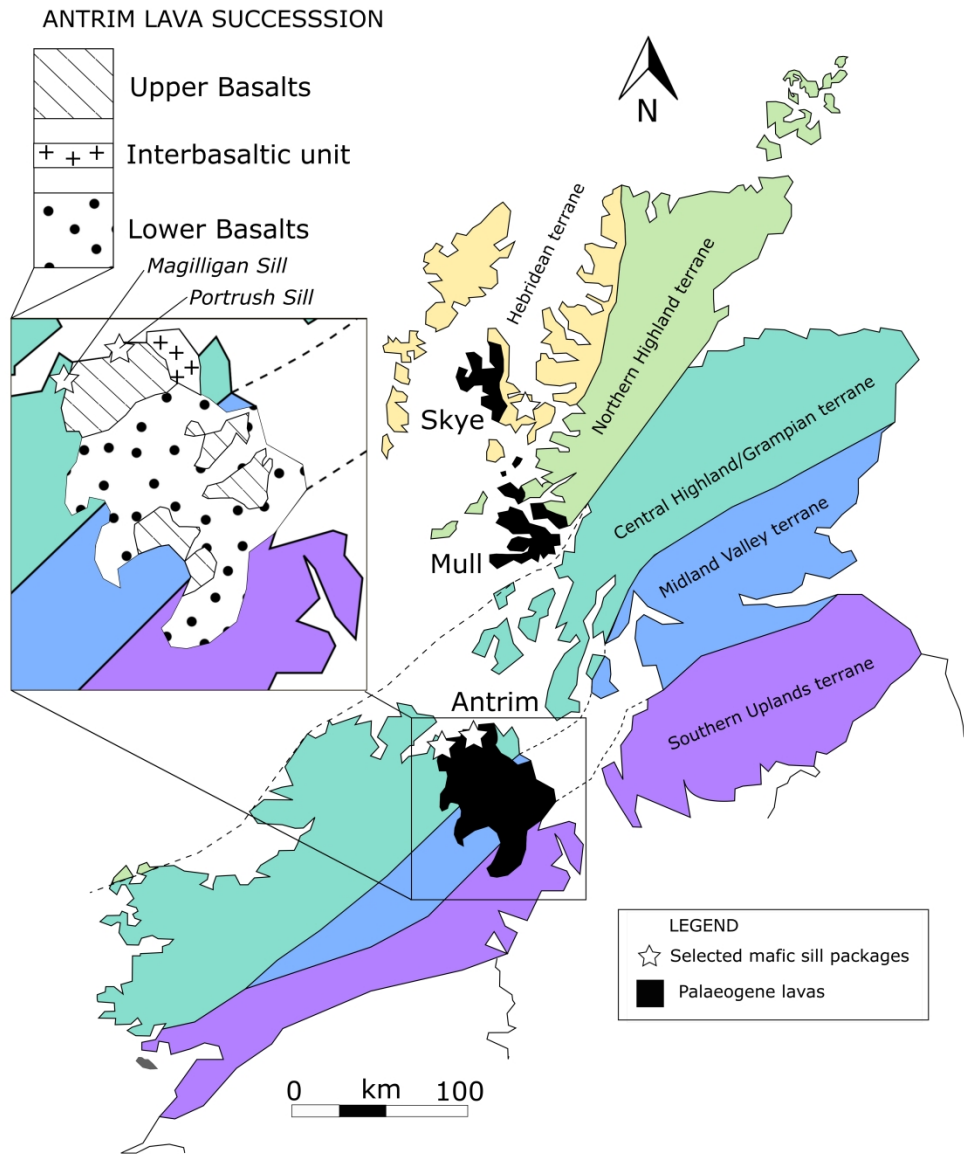


Figure 1 – Schematic map of the geology of the BPBP, showing basement units, onshore lavas and notable intrusive complexes. Inset map gives the subdivisions of the Antrim Plateau lavas and the location of the Magilligan and Portrush Sills. Based on work by Woodcock and Strachan (2012).

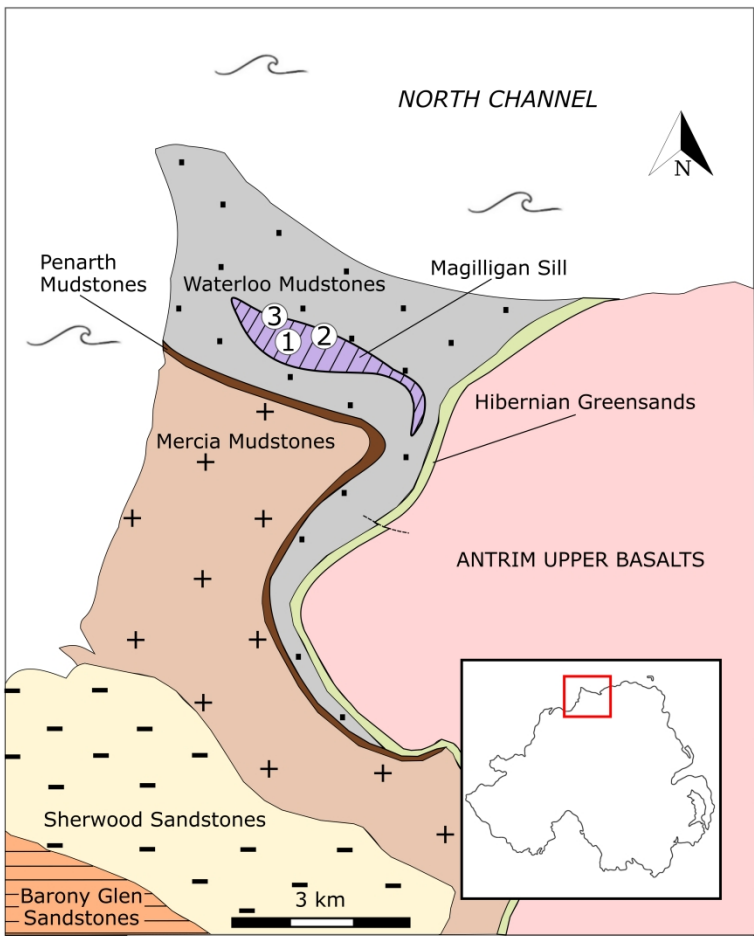


Figure 2 – Schematic geological map of the Magilligan Peninsula, Northern Ireland, indicating the location of the Magilligan Sill and Boreholes 1-3.

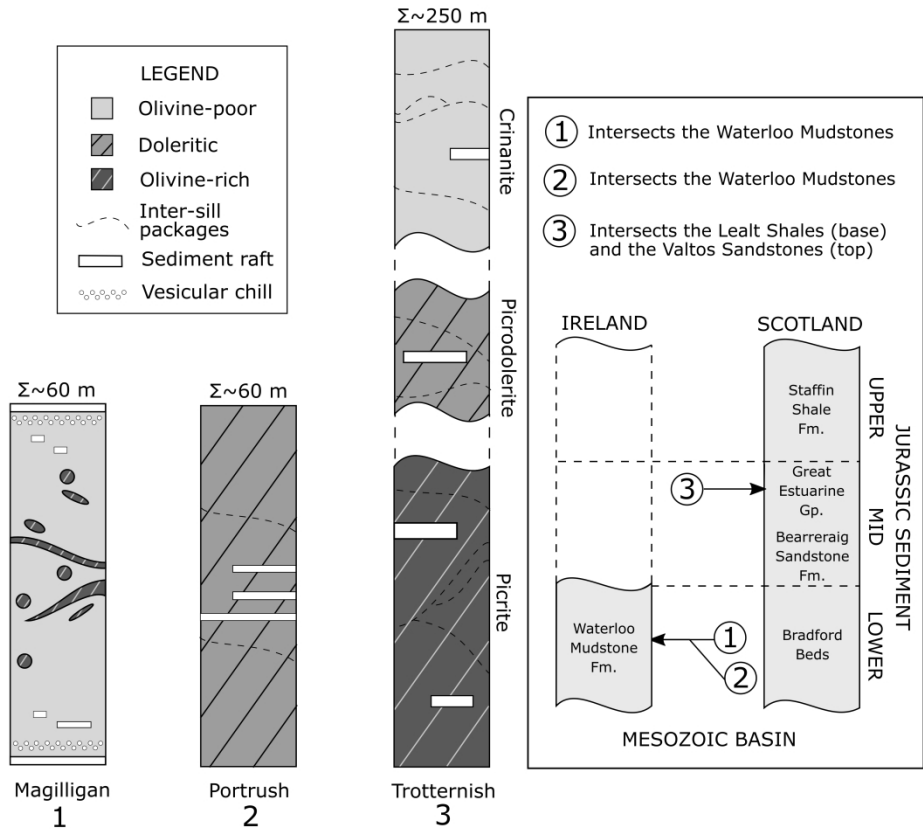


Figure 3 – Simplified lithological logs of the Magilligan, Portrush and Trotternish Sills, with their relative intrusion level within the Jurassic stratigraphic columns for Scotland and Ireland. Sill packages are stylised to show multiple injection events. Formation names from Woodcock and Strachan (2012) and GSNI (2004). Portrush and Trotternish relationships from Ledevin (2012), and Gibson and Jones (1991), respectively.

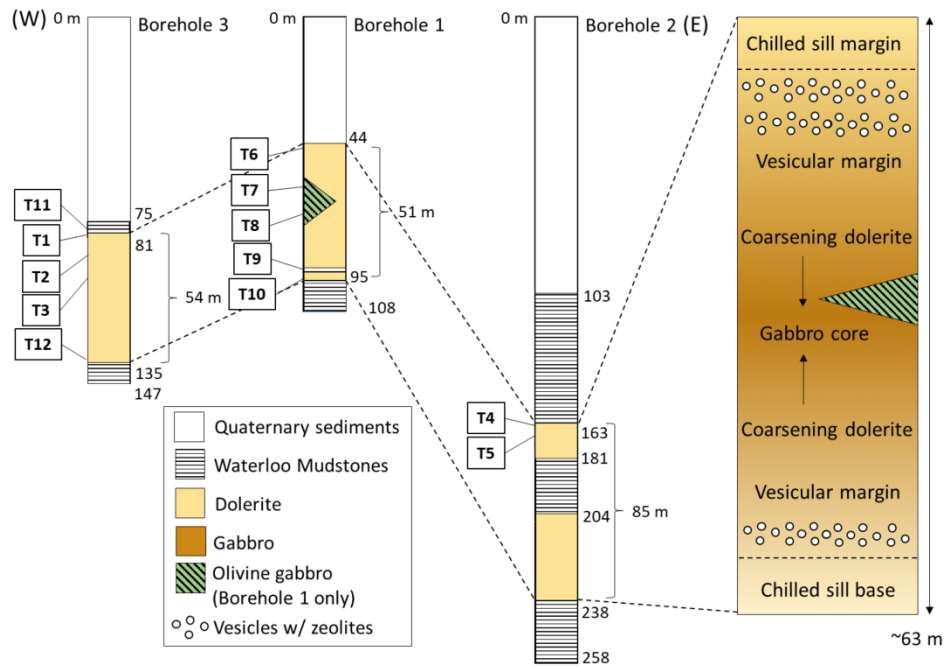


Figure 4 – Representative composite geological log of the Magilligan Sill boreholes. "T" labels show the analysed thin section sample numbers and locations.

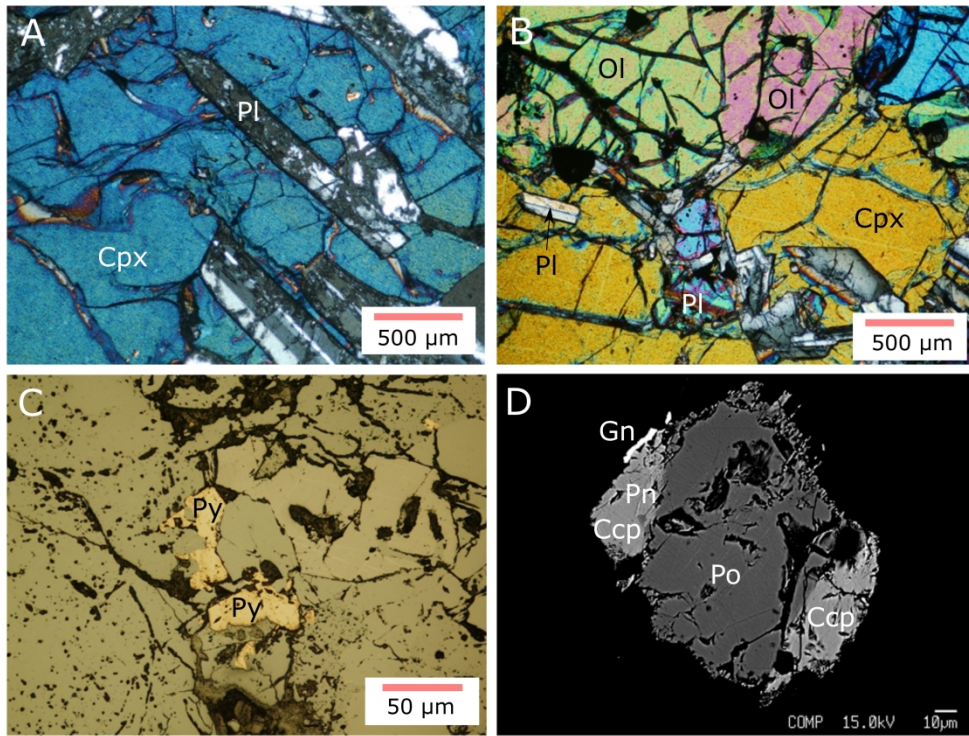


Figure 5 – Photomicrographs of Magilligan Sill thin sections: a) Olivine-deficient gabbro (T3) [transmitted light XPL]; b) Olivine gabbro (T7) [transmitted light XPL]; c) Small pyrite grains within gabbro (T2) [reflected light]; d) Large sulphide amalgamation within olivine gabbro, [back-scattered electron image, BSE] (T2). [Pl – plagioclase, Cpx – clinopyroxene, Ol – olivine, Py – pyrite, Po – pyrrhotite, Ccp – chalcopyrite, Pn – pentlandite, Gn – galena]

927x729mm (144 x 144 DPI)

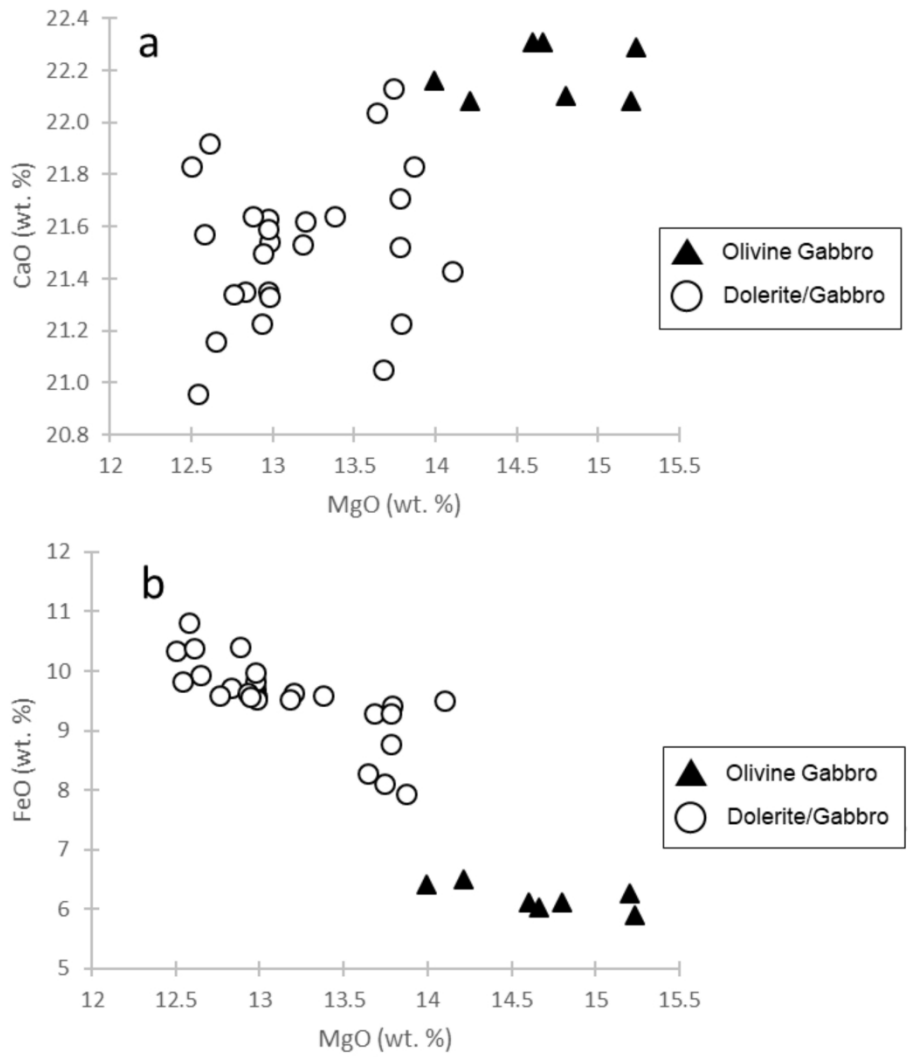


Figure 6 - Bivariate geochemical plots of a) MgO vs. CaO and b) MgO vs. FeO in analysed clinopyroxenes.

465x524mm (144 x 144 DPI)

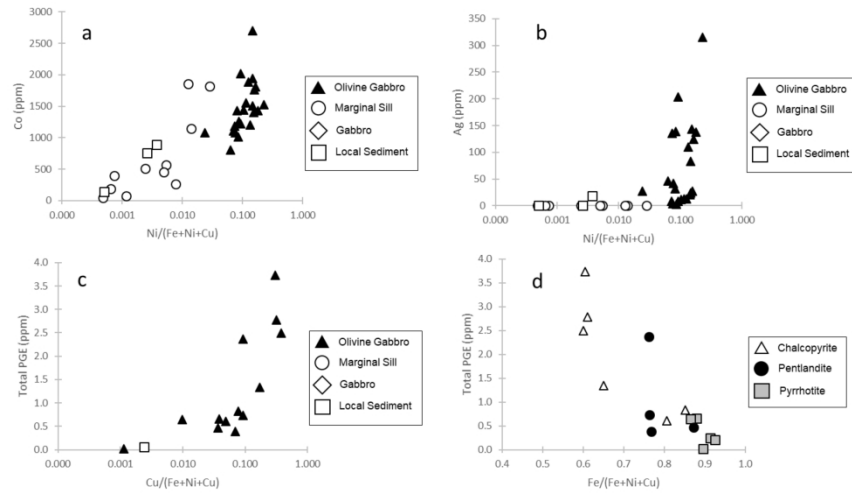


Figure 7 – Bivariate geochemical plots of sulphides in the Magilligan Sill: a) Ni vs. Co; b) Ni vs. Ag; c) Cu vs. total PGE; d) Fe vs. total PGE with respect to mineral phases. Gabbro samples do not contain detectable Ni or PGE.

881x513mm (144 x 144 DPI)

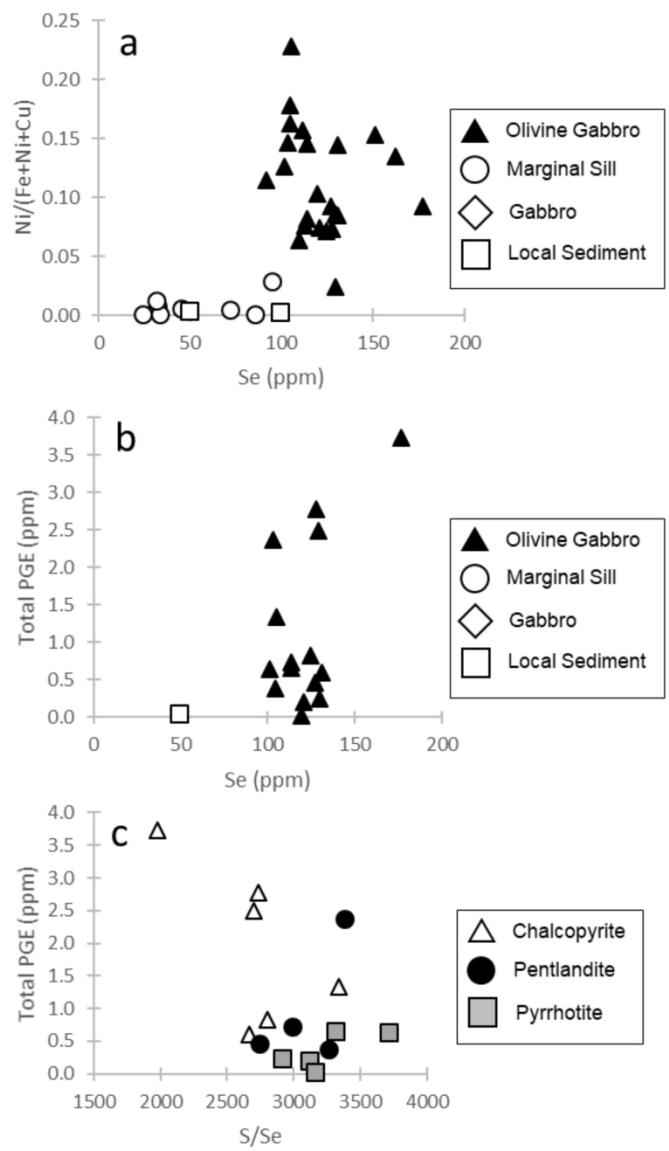


Figure 8 – Bivariate geochemical plots of sulphides in the Magilligan Sill: a) Se vs. Ni/(Fe+Ni+Cu); b) Se vs. total PGE; c) S/Se vs. total PGE with respect to mineral phases.

399x649mm (144 x 144 DPI)

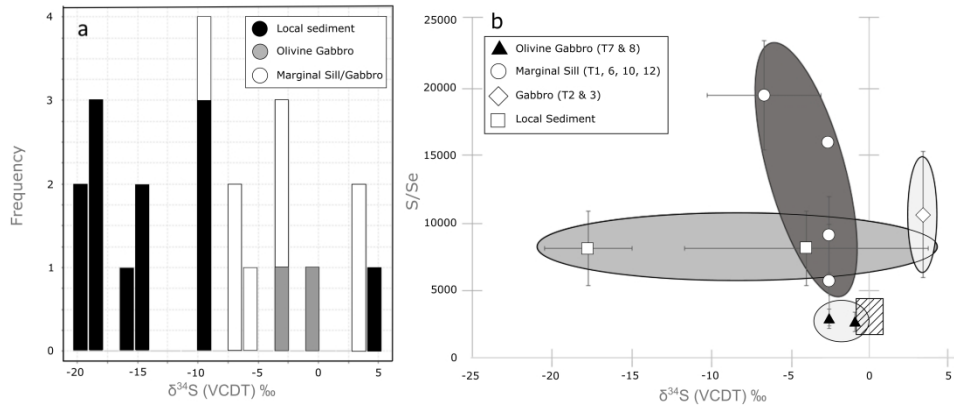


Figure 9 – a) Histogram of $\delta^{34}\text{S}$ compositions of sulphides in the Magilligan Sill. b) Combined $\delta^{34}\text{S}$ vs. S/Se plot for sulphides in the Magilligan Sill, with published magmatic values from Seal (2006) and Quefferus and Barnes (2015). Crosshatched area represents typical magmatic/mantle values.

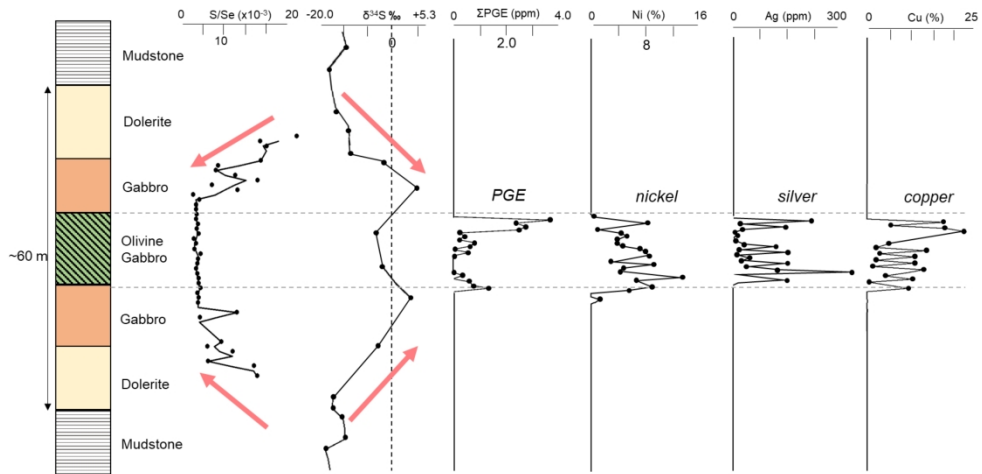


Figure 10 – Representative downhole variations in lithology (not to scale) combined with S/Se, $\delta^{34}\text{S}$, total PGE, Ni, Ag and Cu data from sulphides in these lithologies. Arrows on S/Se and $\delta^{34}\text{S}$ plots describe the suggested diffusion profile grading inwards from dolerite to gabbro.

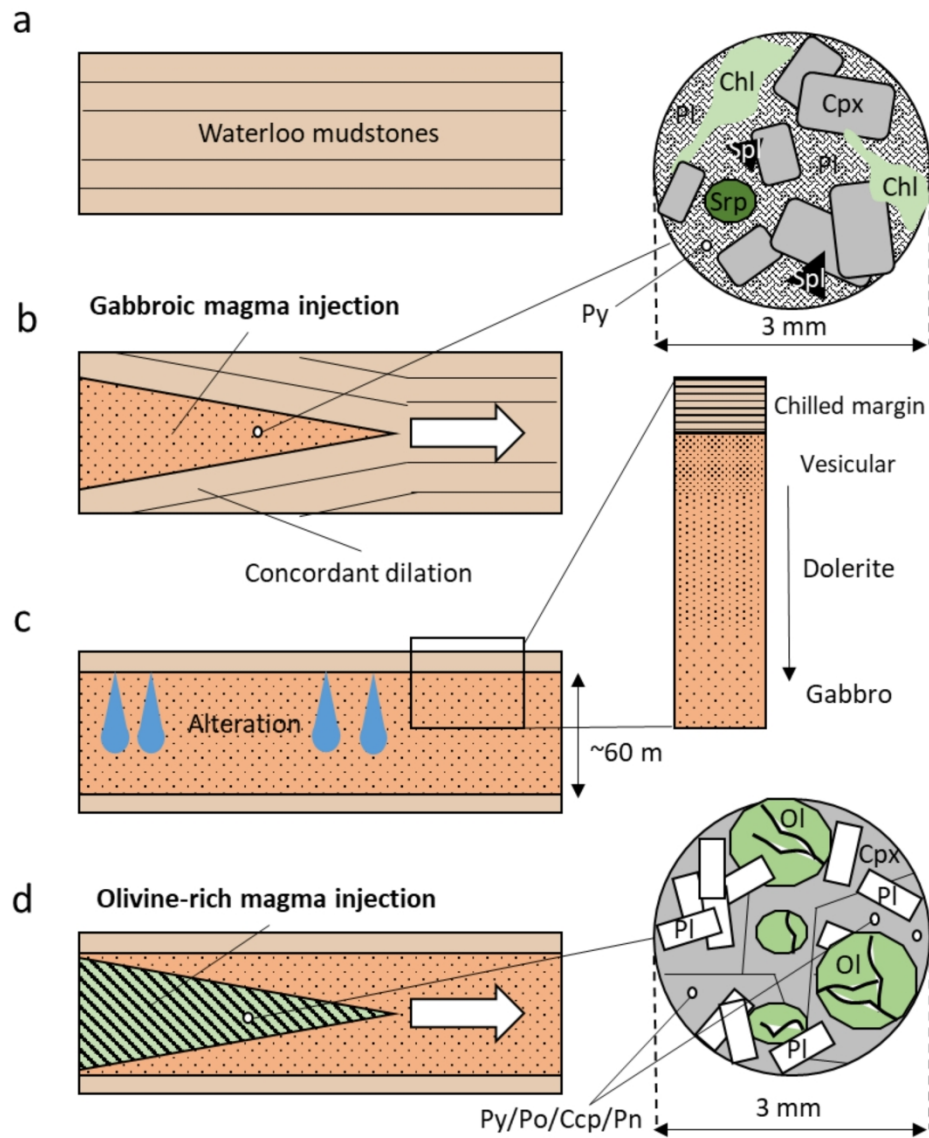


Figure 11 – Petrological development of the Magilligan Sill, showing the two lithological phases found in the intrusion. [Pl – plagioclase, Cpx – clinopyroxene, Ol – olivine, Srp – serpentine, Chl – chlorite, Spl – spinel, Py – pyrite, Po – pyrrhotite, Ccp – chalcopyrite, Pn – pentlandite]

729x895mm (144 x 144 DPI)

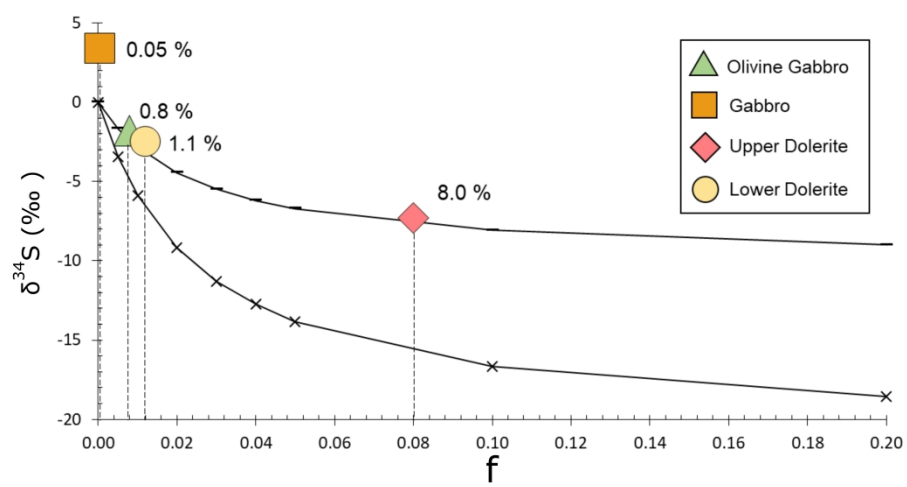


Figure 12 – Binary mixing model for the Magilligan Sill and sedimentary sulphur.

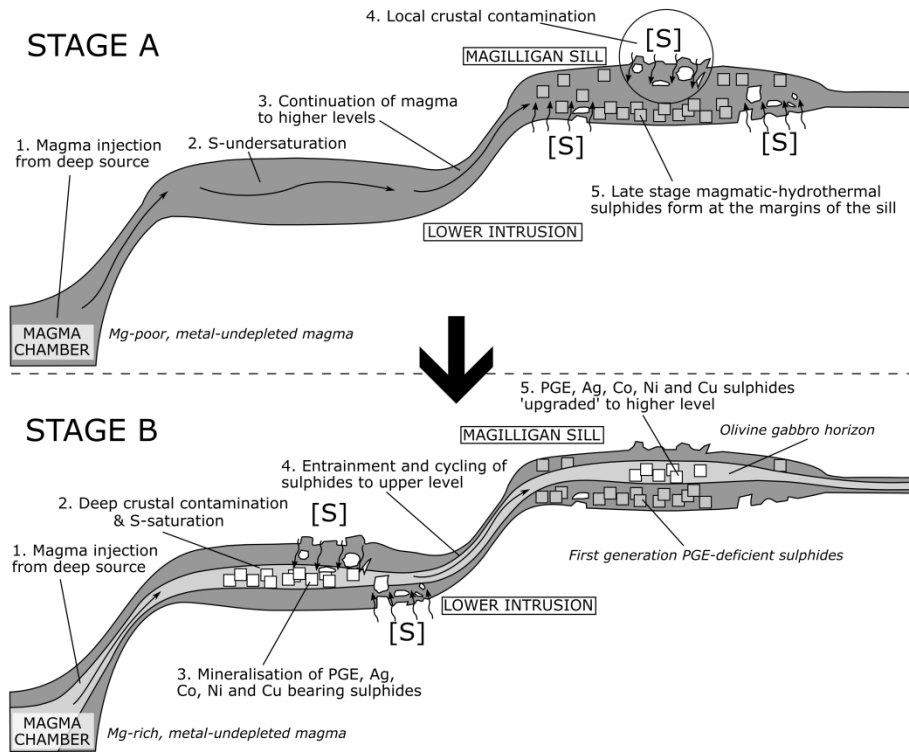


Figure 13 – Stage A in the magmatic development model for the Magilligan system, showing the formation of the dolerites and gabbros, and their barren sulphides. Stage B in the magmatic development model for the Magilligan system, showing the formation of the olivine gabbros, and their cycled base/precious metal sulphides. Model constructed with reference to similar systems in Barnes et al. (2016).